Title
Probing E-cadherin-Mediated Cell Adhesion Using Supported Lipid Bilayers

Author
Hartman, Kevin Laurence

Publication Date
2013

Peer reviewed|Thesis/dissertation

Probing E-cadherin-Mediated Cell Adhesion Using Supported Lipid Bilayers

by

Kevin Laurence Hartman

A dissertation submitted in partial satisfaction of the
requirements for the degree of
Doctor of Philosophy

in

Chemistry

in the

Graduate Division

of the

University of California, Berkeley

Committee in charge:

Professor Jay T. Groves, Chair
Professor David Chandler
Professor David Drubin
Professor Ke Xu

Fall 2013

Probing E-cadherin-Mediated Cell Adhesion Using Supported Lipid Bilayers

Abstract

Probing E-cadherin-Mediated Cell Adhesion Using Supported Lipid Bilayers

by

Kevin Laurence Hartman

Doctor of Philosophy in Chemistry

University of California, Berkeley

Professor Jay T. Groves, Chair

The E-cadherin cell adhesion protein is important for embryo development and cell-cell junction stability, and furthermore plays a role in tumor suppression. It binds apposing cells by forming trans-dimers, which can additionally be stabilized by cis-interactions. However, given the low affinity of the trans-dimer, questions persist about the mechanisms that drive the assembly of such biologically important junctions. One recent theory describes the cooperation of trans and cis-affinity in stabilizing contacts of freely diffusing E-cadherin. Another theory is instead based on the force dependence of different trans-dimer configurations. Not to be overlooked, any such hypothesis must also consider the influence of actin dynamics in forming stable junctions. A synthetic cell membrane platform was used to address these concerns by creating a controlled environment for observing E-cadherin interactions on the planar surface of a supported lipid bilayer. This allowed for the precise adjustment of physicochemical attributes and direct observation of E-cadherin mediated assembly, which uncovered new aspects of adhesion regulation.

The behavior of cells with E-cadherin has been studied previously using lipid bilayers, but such experiments have lacked even a minimal physical characterization of the membrane surface and direct imaging of cell interactions. In this study, an E-cadherin bilayer platform was characterized with respect to fluidity and density. With the introduction of the epithelial cell line MKN28, cells were observed to interact and transport the E-cadherin, causing enrichment of the protein above initial bilayer surface densities. Immunostaining these cell-bilayer interfaces exposed an architecture similar to those found in vivo, suggesting the formation of mature E-cadherin mediated adhesions.

The current system led to the observation that cells assembled junctions on a low-mobility protein surface much more frequently than with a fluid bilayer (adhesions assembled in 54% of cells vs. 1%). Limiting protein fluidity in other ways, such as using nano-patterned diffusion barriers, non-fluid bilayers, and cross-linking antibodies, only showed enrichment events with 1 – 3% of the cells added. The reason for this unusual behavior comes from the physical response between the surface and the cell's retraction of filopodia during junction formation.

Cells on both fluid and low-mobility surfaces exhibited active membrane protrusions, but only on the low-mobility surface was protein enrichment observed underneath retracting filopodia.

This discovery shows that E-cadherin adhesions are formed by an active process, which is dependent on the force and densities resulting from interactions with the low-mobility lipid surface. These lipid bilayer studies address the theories of adhesion assembly, with results suggesting that the decreased diffusion of E-cadherin on the low-mobility lipid surface provides the stability and resistance needed for the formation of robust, force-dependent junctions.

To my Parents

About the “whaling voyage” … It will be a strange sort of book, tho’, I fear; blubber is blubber you know; tho’ you may get oil out of it, the poetry runs as hard as sap from a frozen maple tree; — & to cook the thing up, one must needs throw in a little fancy, which from the nature of the thing, must be ungainly as the gambols of the whales themselves. Yet I mean to give the truth of the thing, spite of this.

—HERMAN MELVILLE, LETTER TO RICHARD HENRY DANA JR., 1 MAY 1850

Contents

List of Figures

List of Tables

Acknowledgments

I'm thankful to Professor Jay Groves for providing the initial project idea and financial support for the work in both Singapore and Berkeley, as well as his guidance and patience for the duration of the entire project.

Professor Ronen Zaidel-Bar, Cheng-han Yu, and Zhenhuan "Gary" Guo supplied valuable technical insights and constructive criticisms, as well as collaborating professors Lawrence Shapiro and Barry Honig.

Kabir Biswas helped immensely in keeping the project moving after my struggle with years of negative results with E-cadherin constructs, as well as technical assistance in molecular biology techniques, microscopy/FCS, data analysis, and keeping up to speed on the scientific literature.

Technical assistance directly related to the project also came from Wan-chen Lin, William Huang, and Adam Smith. Oliver Harrison and Julia Brasch from the Shapiro Lab provided the initial 568-Ecad-H12 protein and information on its purification.

On the Berkeley side, Khalid Salaita, Pradeep Nair, Adrienne Greene, Elizabeth Xu, Michael Coyle, Samuel Lord, Hector Huang, Niña Caculitan, and Nicole Fay have helped at one time or another in techniques or advice. In the Mechanobiology Institute, similar help came from Megha Rao and Aishwarya Srinivasan.

Though not technically a part of the research project, I also must acknowledge Professor Ke Xu's alacrity to become a committee member very late in the semester. I am very grateful for his help.

Chapter 1

Cadherin-mediated cell-cell adhesion

1.1 Why cell-cell adhesion matters

In the most basic sense, cell-cell adhesion is the principal characteristic separating single-cellular species from multicellular organisms. As one may expect, it is an important factor of embryogenesis, as well as any other biological process that involves geometric rearrangement, such as wound healing, epithelial cell migration, cell sorting, and growth. Interestingly, cell adhesion must allow for some degree of dissociation between adhering cells, rather than acting as a permanent glue. But in the development of cancerous tumors, too little cell adhesion has been observed, leading to metastasis and an increase of invasive properties [1, 2].

1.2 Cell adhesion by the cadherin molecule

Cadherin is the most prominent cell-cell adhesion protein, and is enriched at sites of cell-cell contact in epithelial tissues. It was originally discovered by Takeichi in 1977 when he noticed that there were two types of adhesions formed between Chinese hamster V79 cells: one type dependent on calcium and the other type independent. The calcium-dependent adhesion was protected from trypsinization whenever Ca^{2+} remained in the media, and this interaction was nailed down to a 150 kDa protein, which became known as a cadherin protein [3, 4]. In cell culture and with cadherin coated surfaces, such as beads or vesicles, chelating the calcium from solution will cause dissociation without the enzymatic cleavage induced by trypsin. This calcium dependence of cadherin is routinely exploited as a reversible "calcium switch" in experiments to disable and restore the cadherin-dependent adhesion. Disabling the adhesion is done by washing a tissue monolayer or beads with a metal chelating solution (usually containing EDTA or EGTA), and the adhesion is restored with a Ca^{2+}-containing solution (normal cell media is sufficient) [5–7].

The main subfamilies of vertebrate cadherins are distinguished through their strand-swapping mechanism. Type I cadherins include E, N, P, and C-cadherin, which all have five extracellular domains and form calcium-dependent W2 strand-swapped homodimers. Type II cad-

herins have a similar structure with Type I but strand-swap an additional tryptophan (W4) in addition to the W2. This subfamily includes VE-cadherin and Cadherin-11 [8]. Type I cadherins cannot bind Type II, but the structures are similar enough within those subfamilies to allow promiscuous binding. It has been observed that the three cadherins E, N, and C, even of different species, are able to bind among themselves, forming hetero-dimers with dissociation constants that are only slightly different than those of homodimers [9, 10]. However, cells expressing primarily one or the other of these cadherins can sort out from a mixture, forming clusters of cells that express the same cadherin.

Cadherins—by definition, the cell adhesion glycoproteins that require calcium for binding—include several other proteins within the subfamilies of desmosomal and proto-cadherins, as well as other non-classified cadherins [8]. However, this paper will focus on a single member of the cadherin family, E-cadherin, which has been studied in depth more than the other cadherins.

1.2.1 Structure and binding of extra-cellular E-cadherin

E-cadherin is a transmembrane glycoprotein with five extracellular (EC) domains, and is the main component of cell-cell adhesion in epithelial cell monolayers (hence the "E"). The first domain, EC1, contains a tryptophan (W2) as the second amino acid in sequence, and this residue is vital for the formation of trans-dimer formation as a point mutation to an alanine (W2A), prevents it. This is because the mechanism of the bond, called *strand-swapping*, involves the W2 strand of one protein to swing out of its hydrophobic pocket within EC1 and nest inside that of its binding partner, with the binding partner undergoing the same conformational change (see figure 1.1). Analytical centrifugation shows the K_D of this strand-swapped dimer of human E-cadherin to be 217 ± 30 μM at 37°C[11]. Compared to other non-cadherin adhesion proteins, this suggests weak binding. For example, the K_Ds between monomeric ephrin ligand and Eph receptor, and of integrin with fibronectin, are on the order of nMs, corresponding to higher affinities [12, 13]. E-cadherin trans-binding may have a lower affinity in order to permit a certain degree of tissue remodeling.

The strand-swapping mechanism is also how calcium-dependence works allosterically. Calcium binding pockets exist between each of the five domains, and the presence of calcium in these pockets increases the rigidity of the protein at those connections. Structural and simulation studies show that calcium binding between the EC1 and EC2 domains allows the W2 strand to pivot outside of its hydrophobic pocket and be available for strand-swapping[9]. This pivoting relies on a salt bridge created by the interaction of the residue E89 with Ca^{2+}. Without the calcium, or with a mutation like E89A to disable salt bridge formation, the W2 strand does not pivot and is thus not available for trans-dimer formation .

Strand-swapping, however, is only one mode of trans-dimerization. Structural studies have revealed a cross-dimer (X-dimer) as an intermediary, lower affinity state that occurs before an apposing pair of E-cadherin molecules form strand-swapped dimers. This X-dimer state has been observed in crystal structures of E-cadherin mutants, such as W2A, in which stand-swapping is inactivated, but proteins form a trans configuration, with dissociation constants

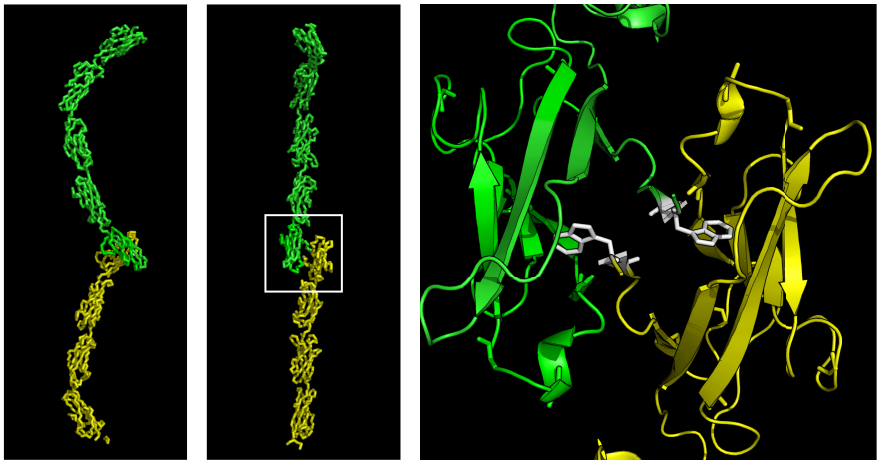

Figure 1.1 – Extracellular E-cadherin domains in strand-swapped trans-dimer configuration. The rightmost panel zooms in on the square of the center figure, illustrating the strand-swapping of the W2 side chains (colored white). This structure is the version of mouse E-cadherin, with the exception of the mutations C9S and C532S, used in the experiments of the next two chapters. Image created from PDB structure 3Q2V featured in Harrison et al. [14].

a magnitude higher than WT E-cadherin [15]. This weak X-dimer structure involves a parallel configuration of the protein with a close contact formed with the residues between EC1 and EC2, especially involving residue K14. Mutations of this lysine, such as K14E, lead to a protein that forms strand-swapped dimers with a similar K_D as WT E-cadherin. However, this K14E mutant undergoes a slower exchange between monomers and dimers than WT. This change in kinetics seems to be important biologically, as cells transfected with K14E mutated E-cadherin show low levels of aggregation, on par with W2A E-cadherin mutated cells or WT cells in the presence of EDTA [15]. A double mutation against both strand-swapped and X-dimer (W2A, K14E) results in monomeric E-cadherin with no binding tendency.

Another dimer of importance is the cis-dimer, which was previously thought to be the functional unit of E-cadherin adhesion, meaning that the protein must form cis-dimers in order to bind through any trans-configuration. In solution, the K_D of the cis-dimer is on the order of 1 mM, which is too weak to be detected by analytical ultracentrifugation [14]. However, protein K_Ds determined in solution do not match those at play on a fluid surface like a cell membrane, where lateral interactions can be magnified. Also, it has been observed in structural studies that the cis and trans-dimer interactions are not exclusive of each other, and the stability of the trans-dimer increases the probability of cis-interactions [14]. Simulations suggest that the co-operative cis and trans interactions drive the enrichment of E-cadherin at sites of cell adhesion[16, 17]. In chapter 2, this study will confront the question of the protein's oligomerization state on a synthetic membrane surface, which addresses the role of the cis-interactions, absent trans-dimerization and cytoplasmic forces.

1.2.2 Intercellular domain and linkage with the cytoskeleton

Type I and II cadherins are all expressed on the cell surface as transmembrane proteins. The intercellular domain of E-cadherin supplies the connection with the cytoskeleton, which enables the translocation of E-cadherin, This gives cells some ability to modulate the surface density of E-cadherin at adhesion sites, as well as linking the strength of the adhesion with the rest of the cell. Unlike the extracellular domain, this intercellular domain is mostly unstructured, and interestingly, the association with the actin cytoskeleton is believed to occur indirectly: β-catenin binds to the intercellular domain, and monomeric α-catenin binds to that. The α-catenin in this complex is unable to bind to actin simultaneously. However, dimeric α-catenin is able to bind to the actin filament, but not to β-catenin [18, 19].

Because of this indirect connection created by the asymmetry of the α-catenin dimer, clusters of cadherin, even at sites of adhesion, can remodel dynamically, and have been observed to even jump from one actin fiber to the other [20]. Some have postulated that the intercellular domain, dissociating from actin, releases β-catenin. This β-catenin is then free to amplify the activity of the Wnt signaling pathway, and thus increases the cell's tumorigenicity [21, 22]. The intercellular domain can also associate to filamentous actin through p120 catenin and other less studied binding partners [23]. To better understand the role of the intercellular domain, research has been performed with tailless E-cadherin mutants, meaning E-cadherin without the β and p120 catenin binding domains. In cells where the only cadherin expressed was a tailless E-cadherin mutant, adhesion junctions were formed as with WT E-cadherin. Furthermore, the cells showed no morphological defects compared with cells expressing the endogenous E-cadherin [24].

1.3 Questions of junction assembly

Given the low affinity of the strand-swapped dimer and its transient connection to the actin cytoskeleton, models have attempted to describe how stable adhesions can form between cells expressing E-cadherin on their surfaces. Three prominent models are described as follows.

1.3.1 Actin driven processes

E-cadherin mediated adhesion is understood to be influenced by actin polymerization, both through E-cadherin's intercellular domain which connects with actin binding partners and by its localization in tissues at the actin-rich adherens junction. Live-cell imaging of tissue monolayers shows clusters of cadherin translating within cell-cell contacts and moving between separate actin filaments [20].

Actin activity at the cell membrane surface, in the form of dynamic filopodia and lamellipodia, has been observed to drive the assembly of E-cadherin cell adhesions. For example, in epithelial cells, filopodia tipped with E-cadherin project into and make contact with neighboring cells, forming a zipper-like adhesion pattern [25, 26]. Similar behavior has been observed in other cell types and by actin-rich lamellipodia [27]. These contacts are believed to stabilize

initial contacts by a positive feedback loop by local signaling events: E-cadherin accumulated at the membrane recruits PI3-kinase and Rac1, which promote actin polymerization. This flattens the contact area, which increases the opportunity for more E-cadherin binding with the apposing surface, and thus, more PI3-kinase and Rac1 recruitment [28].

While important biologically and easy to observe, the actin driven processes described do not address the molecular level details of E-cadherin adhesion formation. These specifics are considered by the next two models.

1.3.2 Diffusion trap model

Vesicles with E-cadherin have been observed to bind to each other or to bilayers with E-cadherin, suggesting that cells may be able to form E-cadherin junctions without active processes. Earlier experiments by Puech et al. and Fenz et al. have shown that GUV (giant unilamellar lipid vesicles) decorated with the extra-cellular domain of E-cadherin can form adhesions with an E-cadherin functionalized supported lipid bilayer [29, 30]. However, neither group looked at the fluidity of the surface or enrichment of surface density—the readout for GUV+SLB adhesion was solely through reflection interference contrast microscopy (RICM), which showed the proximity of the GUV with the bilayer surface.

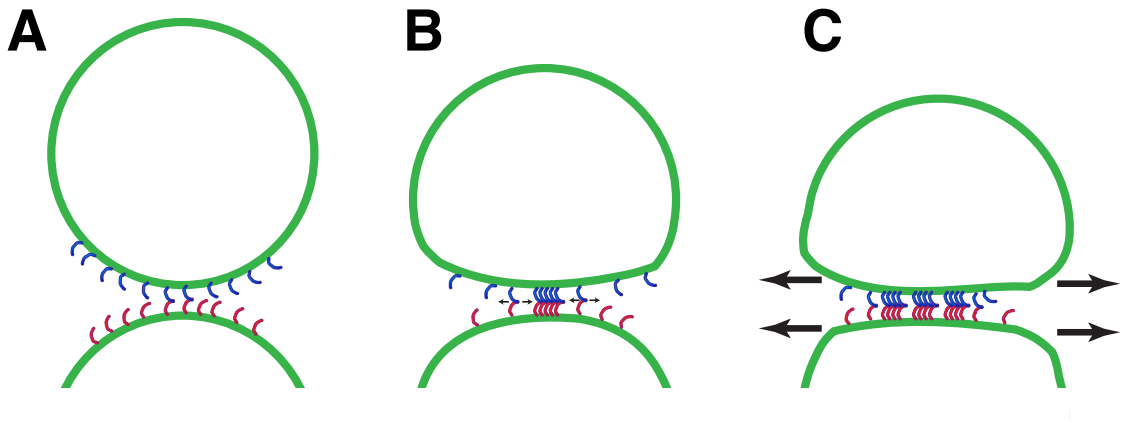

Figure 1.2 – Diffusion trap model. In **A**, two cells or vesicles with diffusing E-cadherin form single, short-lived trans-interactions. A small population of trans-dimers come together and are stabilized by cis-interactions, in **B**. This stabilized contact region allows single trans-dimers to diffuse into the contact region, and become "trapped" by the stabilizing cis-interactions. The cis-interactions, though weak in bulk solution, have a greater influence on a confined surface. In **C**, the contact area grows, and the adhesion strength between the surfaces is increased.

Previously published data by Harrison et al. show adhesion between 100 nm diameter lipid vesicles densely coated with E-cadherin. E-cadherin-H12 was attached to these vesicles of 10% Ni-NTA-DOGS and 90% DOPC, which then showed adhesion by forming ordered cross-sections of protein in vesicle-vesicle adhesions visible by cryo-EM. In contrast, the W2A and K14E trans-dimerization inactive mutants showed disordered junctions. Light scattering analysis of the

vesicles also showed that the wild-type form of the protein led to aggregated vesicles while the trans-dimerization mutants did not [14].

The binding between apposing surfaces of passively diffusing E-cadherin can be described by the diffusion trap mechanism, which explains how an initial contact with only a few E-cadherin trans-dimers to start with can nucleate a stable, enriched E-cadherin junction (see figure 1.2). Through simulations based on the strand-swapped structure, and its trans and cis-affinity, Wu et al. showed that the cooperative nature of E-cadherin binding is key for the formation of enriched junctions [16]. When just a few E-cadherin trans-dimers are formed, E-cadherin monomers on apposing surfaces are able to diffuse towards each other and form the relatively weak strand-swapped trans-dimers. Some of these trans-dimers will separate, but others will diffuse towards the existing adhesion plaque and form stable contacts by the cis-interactions. Though the K_D of the cis-dimer is close to or greater than 1 mM, which describes very low affinity binding, the simulations of Wu et al. show that it is nonetheless necessary for the stability of the E-cadherin adhesion. This is because the confined environment of a 2-D contact region allows the cis-dimerization to stabilize the trans-dimers with a greater effect than in a 3-D solution environment. And thus, with a sufficient starting density and the cooperation of cis and trans-interactions, a stable E-cadherin contact is formed between the two surfaces.

1.3.3 Force dependence in the evolution of binding configurations

The force dependence in E-cadherin trans-dimerization has recently been investigated by Rakshit et al, with the findings summarized in figure 1.3. In their experiments, both an AFM tip and a solid surface were coated with E-cadherin monomers at a specific density, which allowed them to measure the lifetimes of single trans-dimers at different forces [31]. When the strand-swapped dimer arrangement was inactivated by a W2A mutation, or by adding free tryptophan to the buffer, only the X-dimer could form. Rakshit et al. observed the X-dimer to exhibit catch bond behavior up to 30 pN, upon which it changed to a slip bond[1].

Another important observation of the same Rakshit et al. study was the time dependence of strand-swapped dimer formation. When the E-cadherin coated AFM tip was allowed to contact a E-cadherin surface for 3.0 s, slip bonds were formed, which is characteristic of strand-swapped trans-dimers (in this case, the E-cadherin is WT, and there is no tryptophan added to the buffer). But when the contact period was decreased to 0.3 s or less, only ideal bonds were formed, which is characteristic of a weakly binding intermediate between the X-dimer and the strand-swapped dimer [31].

In relation to cells forming E-cadherin adhesions with each other, the force dependent model suggests that the initial contacts are composed of the quickly forming X-dimers, which become stronger under force. With neighboring X-dimers to stabilize the site of adhesion, the bonds are able to change through a weak intermediate into the higher affinity strand-swapped configuration.

[1] Slip bonds have decreasing lifetimes as force is increased, while ideal bonds show no change in lifetime. Catch bonds have increasing lifetimes as force is increased.

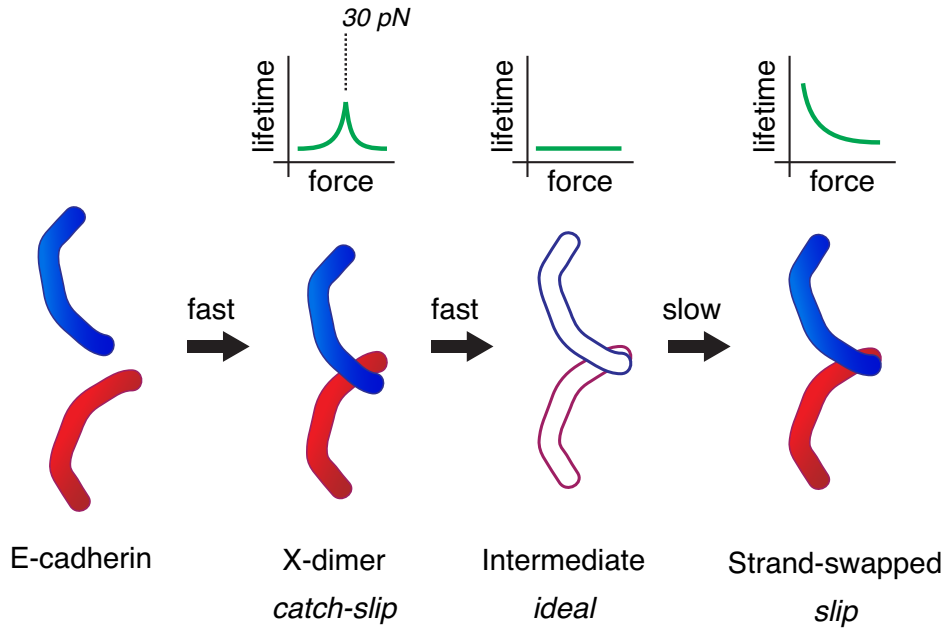

Figure 1.3 – Force dependent binding model from Rakshit et al.[31]. Three modes of trans-dimerization were observed through AFM experiments that probed the strength of single E-cadherin bonds with selective mutations. The model describes that WT E-cadherin monomers first interact through a quickly binding, but weak X-dimer configuration, which has an observed catch-slip bond mechanism with a lifetime that peaks around 30 pN. This is believed to evolve through an intermediate, ideal bond state, into the strand-swapped dimer. The strand-swapped dimer is a slip bond but has higher affinity under low strain than the intermediate or X-dimer. All structures but the intermediate dimer have been solved.

1.4 The supported lipid bilayer as a tool for understanding the binding and assembly of cell surface proteins

To study these contacts in a geometrically and chemically controlled environment, one may restrict E-cadherin to a planar surface, allowing the adhesion of single cells to be fully visualized by optical microscopy. E-cadherin expressing cells have been studied in this manner with surfaces of immobilized protein to investigate cell motility and cross-talk with other adhesion proteins [32]. However, supported lipid bilayers present a more physiologically relevant surface of E-cadherin to adhering cells, as the two-dimensional fluidity of the surface allows protein clustering and transport down to the single molecule scale. Furthermore, previous studies have shown that the restriction of laterally mobile ligands can lead to changes in the cell's signaling pathways that affect the localization of other membrane-bound receptors [33]. On an immobile surface of E-cadherin, cells are unable to reorganize the protein in ways that are significant to signaling and phenotype changes. Thus, while solid non-fluid surfaces of E-cadherin can be a useful tool to quantify cell spreading and mobility, it is not a sufficient platform for simulating

cell-cell interactions.

Flows of cadherin clusters at cell-cell contacts have been observed to have engagement with only one of the cell's cortical actin meshworks, rather than the actin of both cells [20]. And as mentioned previously, cells with tailless E-cadherin mutants are able to form adhesions with one another. These two characteristics support the idea that E-cadherin mediated adhesion of a cell can be reliably simulated with a passive surface that exposes only the extra-cellular domain of the protein.

1.4.1 Previous studies of the E-cadherin decorated membranes and their shortcomings

The previous studies of E-cadherin bilayers and cell interactions must be recapitulated in order to understand the design and goal of the work performed for this dissertation. This overview is not meant to be overly critical of the previous research, but to highlight certain shortcomings that are addressed in this and the following chapters. The technical details of the attachment schemes and fluorescent labels, including some reasons as to why the experiments were not completely successful, are described in the following sections.

One of the earliest instances of attaching E-cadherin to a bilayer occurred in 1999 when Sivasankar et al. attached the extra-cellular domain of the protein to a gel-phase bilayer for the purpose of measuring trans-dimerization forces using AFM [34].This attachment was done using a his-tag, yet the homogeneity of the protein distribution was not checked (though this detail was irrelevant for their application).

Later, in 2004, Puech et al. used a truncated form of E-cadherin (EC1 and EC2 only) with a his-tag to chelate to Ni-NTA lipid head groups within a fluid bilayer[29]. The purpose of the experiment was to observe adhesion with E-cadherin decorated lipid vesicles, which was done using reflection interference contrast microscopy to expose vesicle-bilayer adhesions. Fenz et al. later performed a very similar experiment a few years later, but with the use of the full extra-cellular domain E-cadherin dimer linked to the bilayer through biotin-streptavidin [30]. However, despite their need for fluid E-cadherin surfaces, the constructs of both studies were never fluorescently labeled, which means that Puech and Fenz could not directly check for the protein's fluidity or distribution, including if the E-cadherin was enriched at the sites of vesicle-bilayer adhesion.

The first publication with a fluorescently tagged E-cadherin construct on the bilayer occurred with Perez et al. in 2005. They used a dimeric construct of the full E-cadherin extracellular domain linked to the bilayer by a GPI anchor. However, a dimeric protein may bias cell responses that rely on the formation of membrane protein clusters [35, 36]. The researchers also used the NHS-ester reaction to fluorescently label the lysines on the protein, but this may have disabled trans-binding, as explained in section 1.6.

The next most significant papers are from Andreasson-Ochsner et al. and Charnley et al., which used a protein chain with an antibody to tether dimeric E-cadherin to a bilayer in PDMS

mircro wells [37, 38]. However, the papers never demonstrated the fluidity of the entire protein linkage, and did not show the cells to be binding to and enriching the E-cadherin.

1.5 Attachment schemes: linking proteins to bilayers

The supported lipid bilayer system has originally used the expression of liposome-linked GPI (glycosylphosphatidyl inositol) proteins as a means of connecting a protein with a bilayer [39]. With this procedure, the cDNA encoding the protein includes a signal peptide for the post-translational modification of an alkyl chain to the C-terminus of the protein. This method, however, is technically challenging in that the liposomes must be purified from cells with the protein intact. This not only increases the likelihood of protein degradation but also presents the protein on both sides of the lipid bilayer. This attachment scheme was used in the E-cadherin lipid bilayer study by Perez et al. in 2005 [40], but did not show strong evidence for two-dimensional fluidity.

Another common attachment scheme is the use of a biotin-streptavidin-biotin connection. This is based both on the high affinity of the biotin to the tetrameric protein streptavidin (the strongest known non-covalent bond with a K_D between 10^{-14} and 10^{-16} M [41]), and streptavidin's multiple binding pockets. For bilayer application, a low percentage (typically 0.1%) of biotinylated head group lipids are doped into a fluid bilayer. Streptavidin (or a closely related protein like avidin or neutravidin) is added and links to the bilayer. Then the protein or peptide, which has an added biotin group, is incubated with the bilayer and links to the available binding pockets of streptavidin on the bilayer, completing the linkage. This linkage scheme has been used to successfully create fluid and homogeneous protein-bilayers for cell-cell and cell-ECM proteins to study corresponding cell interactions [33, 42].

However, the method of attaching the biotin molecule to the protein is not a minor detail. The biotinylation procedure typically uses the NHS-ester reaction, which links biotin to the protein's exposed primary amines (specifically, the lysine side-chains). The activity of certain proteins may be dependent on their lysine residues. Biotinylated EphrinA1 ligand appears to retain EphA2 receptor binding activity [33], but biotinylated E-cadherin seems to be non-functional due to the location of lysine residues (see section 1.6 for more). This issue has been circumvented by using a biotinylated IgG antibody to the protein one wants to display, however, adding longer chains of proteins between the bilayer and the protein of interest generally leads to unwanted protein interactions and a decrease in fluidity and homogeneity. The papers Andreasson-Ochsner et al., Charnley et al., and Fenz et al. use this protein chain approach to attach E-cadherin-Fc to an antibody against the Fc domain, which antibody is biotinylated and attached to an avidin-related protein on a biotin-containing lipid bilayer [30, 37, 38]. However, all three papers lack direct evidence of E-cadherin fluidity; Andreasson-Ochner et al. show FRAP data of only a streptavidin-bilayer (the streptavidin is fluorescent), and not of the entire protein linkage.

Lipids with maleimide head groups can also function as a protein-bilayer attachment, but have not been used in any earlier E-cadherin studies. Similar to the biotinylation reaction, the

maleimide reaction is specific to certain protein residues—in this case, the thiol group of cysteines. Instead of attaching to the bilayer, the maleimide reaction has been used to fluorescently tag the E-cadherin construct used in this paper, which has been engineered to include only one cysteine residue. This construct design is discussed further in the next chapter.

The attachment scheme used principally in this study is that of a poly-histidine linkage to a bilayer containing Ni^{2+}. This linkage is the same as that used for the nickel affinity purification of proteins, and consequently, protein attached to the bilayer by the nickel-histidine interaction can be purified in that manner. The Ni^{2+} of the bilayer is held by chelation to the NTA groups (nitriloacetic acid) of a head group lipid. Unlike the tight binding of the biotin-streptavidin complex, the NTA-Ni-Histidine complex is transient, and on a bilayer, his-tagged proteins attach according to different kinetic parameters, as discussed in a previous study [43]. The relevant information is that higher surface densities of protein can be achieved by incubating a small concentration of protein above the bilayer for a longer time, rather than increasing the concentration or trying to shorten the incubation time. This effect is a direct result of the polyhistidine tail's length, which forms more than one chelation to the bilayer Ni^{2+}. Adding more protein leads to a larger population of molecules connected through only one chelation, and not enough space to form more. The optimal amount of protein is something less, in order to allow the molecules to form one chelation, and then the time to form a second or more, which results in a more stably-bound state of the protein. Such a configuration can be stable and fluid for hours. Another advantage of the Ni-Histidine attachment scheme is that there are no linking proteins or chemical reactions required.

Since the snap-tag was not used in this study, but has distinct advantages, its details will be explained in the last chapter as a potential alternative for constructing an E-cadherin lipid bilayer.

1.6 Considerations of fluorescent tagging methods

The NHS ester is a popular reagent for labeling antibodies and some proteins, and has been used to label the extracellular domain of EphrinA1 to study cell-bilayer interactions [33]. However, E-cadherin labeled in that manner shows little or no cell binding activity, as observed in Perez et al. [40] and in this study (table 2.2). From the structure of EC1 at the strand-swapped trans-dimer interface, it is evident that a fluorophore conjugated to an NHS ester likely interferes negatively with E-cadherin binding. This is because the functional group reacts with the primary amines of exposed lysines on a protein, and in the case of EC1, this includes several lysines a number of which are close to the strand-swapping interface (see figure 2.3). A fluorophore conjugated in that location may sterically hinder the strand-swapping mechanism, thus preventing the formation of trans-dimers. Allowing the labeling reaction to run for a shorter amount of time (i.e. under an hour) leads to the conjugation of fewer fluorophores, which may leave a greater population of functional E-cadherin after the reaction. Of course, this runs the risk of leaving more protein unlabeled.

Greater specificity in fluorophore location can be obtained with the genetic fusion of a fluorescent protein, maleimide labeling, or snap-tag. The fusion of a fluorescent protein involves cloning its cDNA into the plasmid of the protein of interest, so that the two proteins express as one, linked together by amino acid sequence. This approach has been used successfully with ICAM-1 and EphrinA1 on the bilayer. The disadvantage is that fluorescent proteins are generally less bright[2] than commercial synthetic fluorophores. Likewise, a significant percentage of the protein may be in a dark state of no fluorescence, due to unfolding or other environmental effects. And from a practical standpoint, the fluorescent protein must be expressed and purified away from light, in order to minimize photo-bleaching. The advantages of the fluorescent fusion protein includes orientation and number: the location of the fluorescent protein is fixed, so there is only a low risk of interference with protein function. With one per protein molecule, statistical analysis to determine oligomeric states (such as with a photon counting histogram) is possible, even with the existence of dark state proteins. This is because there is no way for a single protein molecule to have two or more fluorophores. Fusions of the fluorescent proteins eYFP and mKate2 have been used with the full and truncated extracellular domains of E-cadherin as earlier experiments of this study (see table 2.2), but cells were not observed to bind the protein on fluid DOPC.

As NHS ester (*N*-hydroxysuccinimide ester) is specific to the primary amines of lysine residues, maleimide reagent targets the thiol groups of cysteines. The advantage is that proteins generally have fewer cysteines than lysines, and with careful structural considerations, cysteines can be introduced to the sequence or mutated to different residues in order to create a site-specific label.

[2]lower quantum yield and/or extinction coefficient at fluorescence excitation frequency

Chapter 2

Physical characterization of the E-cadherin lipid bilayer

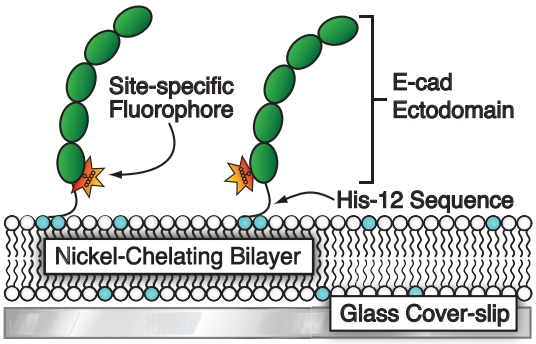

Figure 2.1 – Schematic of 568-Ecad-H12 lipid bilayer. The complete extracellular domain of E-cadherin is displayed on the surface of a bilayer in monomeric form. Site-specific fluorophore and attachment his-tag are located at the C-terminus, in order to allow complete cis-interactions among the proteins (and furthermore trans-dimerization in the presence of cells). The majority of results in the study concern this particular 568-Ecad-H12 construct, which sequence is explained further in figure 2.2.

2.1 Supported lipid bilayer construction

Construction of the protein lipid bilayer involves three main steps: the production of hydrated lipid vesicles, their spreading on a hydrophilic glass coverslip to produce the lipid bilayer, and the addition of protein for attachment to the bilayer surface. The procedure used below is adapted from Lin et al. [39].

2.1.1 Materials

Lipids were purchased from Avanti Polar Lipids, Inc. (Alabaster, AL) or Life Technologies (Carlsbad, CA); table 2.1 lists abbreviated names of the lipids used in this study. From chloroform solutions containing 1 – 5 mg/mL, lipids were mixed in different molar ratios in order to produce bilayers with lipid head groups at specific surface densities. For instance, the main component of the lipids was typically DOPC or DMPC. Ni-NTA-DOGS was typically doped into the lipid mixture at a 4% molar ratio. N-cap biotin was used at a 0.1% molar ratio. Fluorescent lipid probes, if used for surface density calibration or to visualize bilayer coverage and fluidity, were doped into the membrane at mole ratios of 0.1% for NBD-PC, 1% for Marina-Blue DHPE, and 0.001 – 0.05% for Texas-Red DHPE.

These lipid chloroform mixtures totaled 1 mg lipids per sample, and each were contained in 5 mL round-bottom flasks. The chloroform was dried from the lipids by rotary vacuum, and the lipid film was hydrated with 2 mL DI water for a final hydrated lipid concentration of 0.5 mg/mL.

These hydrated lipids adopt different intermolecular configurations, such as giant and multilamellar vesicles and tubular structures. Probe tip sonication was used to break these large aggregates into more useful small unilamellar vesicles (SUVs, ~30 nm diameter [44]) that rupture evenly to form a supported lipid bilayer with homogeneous coverage. Each hydrated lipid mixture was transferred to a small test tube on ice, with the probe-tip lowered directly into the solution. The sonication was performed using a titanium alloy probe tip and sonicator (Sonics Vibra Cell VC750, Sonics & Materials inc, Newton, CT) using 30% power and a 9.9 s ON / 3.3 sec OFF pulse cycle for a total of 2 min 20 s. To remove solid debris from the sonication process, the SUV mixtures were centrifuged at $20,000 \times g$ and 4 °C for 3 – 4 h, and decanted by transferring the top 1.7 mL of each 2 mL sample to a new tube. The lipid vesicles can be stored at 4 °C for up to two weeks before use.

For the actual supported lipid bilayer assembly, glass coverslips of #1 thickness and 25 mm diameter were first cleaned by 30 min sonication in a 1:1 mixture of isopropanol and water. After rinsing with water, the coverslips were then transferred in a Teflon® rack to a fresh piranha solution (3:1 mixture of H_2SO_4 : 30% H_2O_2) for 5 minutes or to an enclosed UV Ozone generator (UV/Ozone ProCleaner Plus, Bioforce Nanosciences, Ames, IA) for 30 minutes. This acid or deep UV treatment breaks apart adsorbed organic molecules and furthermore creates a hydrophilic glass surface by increasing the number of silanol groups (Si-OH) on the surface [45].

Glass coverslips were then rinsed extensively and dried under a stream of N_2 or argon. Lipid vesicles were deposited on the glass by mixing 15 μL lipid vesicles with 15 μL 2 x TBS, and putting the 40 μL solution into a small plastic petri-dish. Then a single coverslip was dropped onto the lipid and TBS mixture, which quickly and evenly spreads the lipid vesicles on the bottom surface of the coverslip. The petri dish and coverslip were then submerged into a container of DI water. The coverslip was lifted out using forceps and gently swirled in the water bath, to remove excess vesicles. While holding the coverslip underwater with the lipid side facing up, the glass coverslip was assembled into an Attofluor Cell Chamber (Life Technologies).

Bilayers and sample chambers were assembled at room temperature, but to ensure consis-

tency with cell results, all bilayer imaging was carried out at 37°C.

Table 2.1 – Lipids used in this study. This table shows the full name and vendor of the lipids used, as well as gel phase transition temperature (source: Avanti), and peak fluorescent excitation and emission, where applicable.

Abbreviated Name	Full Name	Tm	Fluorescence Ex/Em	Vendor
DOPC	1,2-dioleoyl-*sn*-glycero-3-phosphocholine	−20°C		Avanti Polar Lipids
DMPC	1,2-dimyristoyl-*sn*-glycero-3-phosphocholine	23°C		Avanti Polar Lipids
DPPC	1,2-dipalmitoyl-*sn*-glycero-3-phosphocholine	41°C		Avanti Polar Lipids
Ni-NTA-DOGS	1,2-dioleoyl-*sn*-glycero-3-[(N-(5-amino-1-carboxypentyl)iminodiacetic acid)succinyl] (nickel salt)			Avanti Polar Lipids
Biotin-DPPE	1,2-dipalmitoyl-*sn*-glycero-3-phosphoethanolamine-N-(cap biotinyl) (sodium salt)			Avanti Polar Lipids
NBD-PC	1-myristoyl-2-[12-[(7-nitro-2-1,3-benzoxadiazol-4-yl)amino]dodecanoyl]-*sn*-glycero-3-phosphocholine		460/534 nm	Avanti Polar Lipids
Marina Blue DHPE	Marina Blue® conjugated 1,2-dihexadecanoyl-*sn*-glycero-3-phosphoethanolamine		365/460 nm	Life Technologies
Texas Red DHPE	Texas Red® conjugated 1,2-dihexadecanoyl-*sn*-glycero-3-phosphoethanolamine, triethylammonium salt		595/615 nm	Life Technologies

2.1.2 Technique

For protein attachment, the bilayer samples were rinsed with 5 – 15 mL TBS (pH 7.4) and incubated for 5 minutes with 150 nM $NiCl_2$ to saturate the surface binding sites. The samples were blocked with 0.01% BSA in TBS for 30 minutes, and then rinsed with 5 -15 mL TBS containing 1 mM $CaCl_2$, pH 7.4 (TBS+Ca).

The concentrated protein stock of 568-Ecad-H12 (2 μL, 2 mg/mL) was diluted to a volume of 200 μL in TBS+Ca, and half of this was added to each sample containing 900 μL solution, which

was then gently pipetted up and down to evenly mix. The solution above the bilayer is thus a concentration of ~30 nM protein. This was incubated at room temperature for 90 minutes, rinsed with TBS+Ca, and left to incubate for another 20-30 minutes. Following the second incubation step, the sample was rinsed again with TBS+Ca for cell-free bilayer characterization. For cell experiments, the sample was rinsed with an imaging buffer, and the procedure continues in section 3.2 on page 37.

2.2 Designing the protein construct

2.2.1 Protein constructs used

See table 2.2.

Figure 2.2 – The expressed protein sequence of mouse Ecadherin-H12 used in this study. The construct contains the mutations C9S and C532S (green highlighting), which leaves C449 (red highlighting) as the only cysteine available for maleimide fluorophore labeling. The extra-cellular domains are marked by the tan arrows, and EC5 is truncated early by 11 amino acids. The cis-inactivating mutant furthermore contains the mutations V81D and L175D (sites underlined).

[1] Prof. Lawrence Shapiro, Columbia University, NY

Table 2.2 – E-cadherin protein constructs. This table shows the details of the different fusion proteins and constructs used in the study, including the two antibody constructs which will be discussed in Chapter 4. These are roughly in the chronological order used over the course of the dissertation project. *Fluidity on Bilayer* refers to micron-scale fluidity and homogeneous coverage observed by traditional FRAP analysis. *Enrichment by cell* refers to an active process within the cell that increases the surface density of the bilayer-bound protein within the cell's contact region. This can be clustering or a more general increase in fluorescence intensity from the bilayer protein.

Name	**Source**	**Ecad Species**	**Expression**	**Attachment Scheme**	**Fluidity on Bilayer?**	**Enrichment by Cell?**
Ecadherin-Fc	R&D Systems	human	mammalian	his-tag or biotin-streptavidin	N	not obvious
Ecad-mKate2-H10	own	human	mammalian	his-tag	Y	N
Ecad-eYFP-H10	own	human	mammalian with CD33 signal peptide	his-tag	Y	N
EC1-eYFP-H10	own	human	mammalian with CD33 signal peptide	his-tag	Y	N
EC12-eYFP-H10	own	human	mammalian with CD33 signal peptide	his-tag	Y	N
EC12-eYFP-H10	own	human	bacterial with no signal peptide	his-tag	Y	N
biotin-DECMA-1	Abcam	antibody	mammalian	biotin-streptavidin	N	Y
Fab-eYFP-H6	Creative Biolabs	antibody fragment	mammalian	his-tag	Y	N
568-Ecad-H12	Shapiro Lab[1] or own	mouse	mammalian with CD33 signal peptide	his-tag	**Y**	**Y**

2.2.2 Fluorophore incorporation

For the 568-Ecad-H12 construct, the cysteines at residues 9 and 532 were mutated to serines, leaving C449 as the only available residue to react with the maleimide fluorophore. Cysteine residues can be important structurally, for the formation of disulfide bonds in proteins. This possibility was considered for the case of 568-Ecad-H12: an X-ray crystal structure of human E-cadherin with the C9S mutation (PDB 2O72) shows that trans-dimers can form with the normal strand-swapping configuration, and without changing the structure of the cis-binding interface [46]. Thus, it appears that the C9S mutation in the mouse E-cadherin of 568-Ecad-H12 would not alter trans or cis binding affinities.

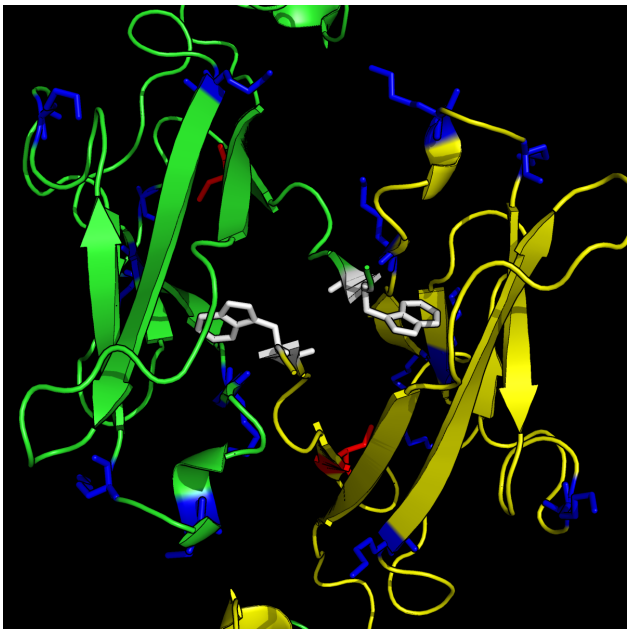

Figure 2.3 – Location of lysines on EC1 within the strand-swapped interface of the mouse E-cadherin trans-dimer. Lysine side chains are colored blue, and in this illustration include K14, K19, K25, K30, K33, K45, K61, and K73. W2 is shown in white, and C9, which is mutated to a serine in the 568-Ecad-H12 construct, is shown in red. Image created from PDB structure 3Q2V featured in Harrison et al. [14].

2.2.3 Purification and labeling of 568-Ecad-H12

The cDNA encoding the 568-Ecad-H12 protein sequence was transfected into HEK-293T cells using the Neon Transfection System (Life Technologies). The cells were grown and selected for protein expression with hygromycin B antibiotic at a concentration of 200 μg/mL in DMEM:F12 media with 10% fetal bovine serum. The cells with the protein expression produce and secrete the E-cadherin-H12 directly into the culture media. After 3 – 4 days the media was exchanged, filtered, and stored at $-80\,^{\circ}$C. After collecting more batches to total 1 – 2 L, the media was thawed, and NaCl added for a final concentration of 300 mM, with the assumption that 150 mM NaCl is originally in the media. Glycerol was added to a final concentration of 10%, and the pH adjusted to 7.4 – 8. The protein was batch purified by adding Ni-NTA agarose beads (Qiagen, Hilden, Germany) into the solution and incubating for 1 – 2 hours at room temperature with gentle agitation. This bead and media mixture was poured into a glass Econo-column (Bio-Rad, Hercules, CA), and the beads were washed with several milliliters of buffer (containing TBS+Ca, 10% glycerol, 20 mM imidazole, pH 7.4). The protein was eluted with a solution containing a high concentration of imidazole (identical to the previous buffer, except with 300 mM imidazole), which effectively competes with the polyhistidine tail for chelation with the Ni-NTA agarose.

Following the crude media purification, the protein solution was concentrated using Vi-

vaspin 2 spin columns, 30 kDa molecular weight cut-off (GE Healthcare, Little Chalfont, United Kingdom), and exchanged into TBS+Ca using PD SpinTrap G-25 columns (GE Healthcare). The protein sample was then mixed with an excess of the thiol-reactive dye, Alexa Fluor 568 C5-maleimide (Life Technologies), in the presence of the reducing agent tris-(2-carboxyethyl)-phosphine (TCEP). This reaction was allowed to proceed for 5 hours at room temperature, with gentle agitation on a nutator or rotisserie turner. The dye reagent was removed by gel filtration chromatography, using a Superdex 200 10/300 GL size exclusion column and the ÄKTApurifier10 FPLC (both GE Healthcare). The column had been equilibrated with a solution of tris-buffered saline, 1 mM $CaCl_2$, and 10% glycerol, with pH 7.4, and the protein was eluted with the same. The eluted fractions corresponding to the peak of absorbance at 280 nm were collected and concentrated using the Vivaspin 2 spin columns. By Bradford assay, the total concentration of protein in the final purified sample was in the range 0.5 – 2 mg/mL. An example of the gel filtration 280 nm absorbance trace and SDS-PAGE analysis of the purified protein is shown in figure 2.4.

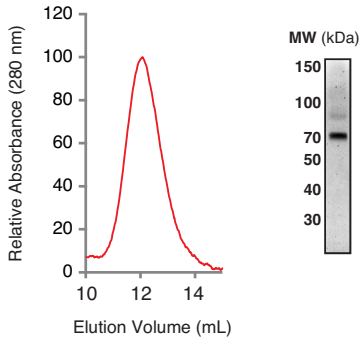

Figure 2.4 – Gel analysis of purified Ecad-H12. Analytical gel filtration shows a single elution peak at 280 nm absorbance, and coomasie stained SDS-PAGE shows a single major band of protein at ~70 kDa, as expected. This confirms that in solution, a wide majority of the protein exists as a monomer.

2.3 Fluidity of the E-cadherin construct on a DOPC bilayer

As the lipids maintain a two-dimensional fluidity, a protein attached to the lipid head groups may also be fluid. Interestingly, for the case of a protein lipid bilayer, the size of the protein does not have a direct, linear influence on the diffusion coefficient: doubling a protein's mass does not guarantee that its diffusion coefficient falls by one-half. Instead, it is the size of the lipid anchor, or the number of lipid molecules associated with the protein's C-terminus, that has the more dramatic effect on diffusion rate [47]. Along with surface density, fluidity is one of the physical properties that cells experience when added to a protein-linked lipid bilayer. Measuring the diffusion coefficient is a way to ensure experimental reproducibility with cell binding

results and to check that the attached protein maintains a homogeneous spread, without extensive oligomerization or the formation of non-fluid defects.

2.3.1 Fluorescence recovery after photobleaching (FRAP)

Imaging the recovery of fluorescence intensity after photobleaching is the easiest diagnostic of bilayer fluidity and homogeneity on the micron-scale, as it can be performed in a matter of minutes on a standard epifluorescence microscope. It involves minimizing the diameter of the field aperture and increasing the excitation intensity of the light to induce photobleaching. After the desired extent of photobleaching, a time series of images are taken with the original excitation intensity and with the field aperture open. An ideal FRAP series taken like this with a fluid bilayer will show a darker, photobleached region that fades evenly outward as photobleached and non-photobleached molecules mix by brownian diffusion. Besides an epifluorescence imaging mode, bilayer FRAP images can also be recorded on a confocal spinning disk microscope that uses a photobleaching module.

Such FRAP image series are taken of a protein attached to the lipid bilayer, or a lipid probe, which is a fluorophore linked to a lipid molecule (and doped into the bilayer at a low mole percent, typically 0.1 – 0.01%). As a single sample can contain both of these fluorescent species, the full micron-scale extent of a sample's fluidity, homogeneous coverage, and aggregation can be observed. A non-fluid bilayer will make for non-fluid bilayer-linked protein. However, the reverse is not always true: the protein can be aggregated to other protein molecules or adsorbed to the glass (sometimes through an existing defect or hole in the bilayer) in a way that does not immobilize bilayer lipids. Figure 2.5 shows a FRAP image of 568-Ecad-H12 linked to a DOPC bilayer containing 4% Ni-NTA-DOGS.

2.3.2 Determining the diffusion coefficient from FRAP images

Quantitative image analysis of the FRAP image series can measure the diffusion coefficient. Firstly, background intensity must be subtracted so that the pixel grayscale value is proportional to the local surface density. Then the global intensity of the images are linearly scaled by some factor to take into account unwanted photobleaching (ie, every image taken confers some amount of decreased image intensity). The diffusion coefficient can be approximated from the recovery of a circular photobleached region by using the simple equation derived by Soumpasis [48],

$$D = \frac{0.224\, w^2}{t_{1/2}}, \tag{2.1}$$

where w is the width of the bleached region and $t_{1/2}$ is the time required for the intensity to recover to half its original value. Using this for a rough estimate with the FRAP image of figure 2.5, w may be assumed as 12 μm, with $t_{1/2}$ in the range of 30 – 45 s. This gives a range of D 0.7 – 1.1 μm^2/s. Of course, more rigorous treatments of diffusion coefficient determination

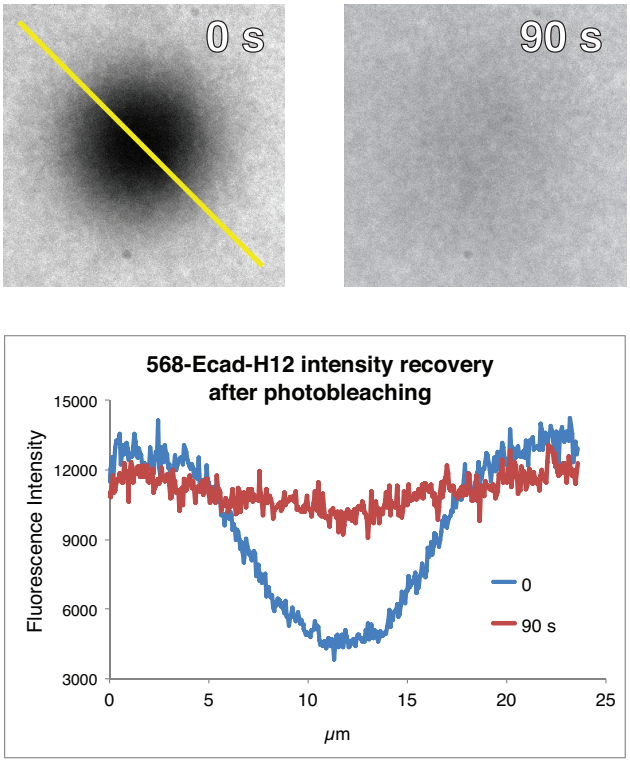

Figure 2.5 – FRAP of 568-Ecad-H12. The complete recovery of fluorescence shows that the protein is fluid on the scale of microns and is linked to the supported lipid bilayer. The image at 0 seconds is taken immediately after opening the field aperture. The line profile through the bleached area further illustrates the fluorescence recovery.

from FRAP intensity profiles exist beyond Soumpasis's approximation (equation 2.1), but most of these require accurate fitting of initial conditions. Solutions can be derived for initial square well or inverted-Gaussian intensity profiles [49]. However, since diffusion occurs in the process of photobleaching a fluid sample, these equations may not perfectly describe initial conditions.

The diffusion coefficient from FRAP images can be determined more rigorously by pixel-wise convolution of fluorescence intensity, which can be applied to any initial condition. Doing this over a range of simulated diffusion coefficients allows one to find the best match between the simulated recovered image and the experimental data, thus finding a global diffusion coefficient from an ensemble of pixel trajectories [49]. This range of diffusion coefficients can be simulated in a MATLAB program written by Raghuveer Parthasarathy and included in Lin et al. [39]. The basis of this program is the fact that both convolution and diffusion can be explained using Fick's laws [50]. This can be demonstrated by starting with a one-dimensional point-wise diffusion process.

For a concentration at an interval i along x, a Taylor series expansion can describe the concentrations of its nearest neighbors as:

$$C_{i\pm1} = C_i \pm \delta x \frac{\partial C}{\partial x} + \frac{1}{2}\delta x^2 \frac{\partial^2 C}{\partial x^2} + \ldots \tag{2.2}$$

Ignoring the higher-order third and following terms, $\frac{\partial C}{\partial x}$ is solved by subtracting C_i from the equation and dividing by δx. This gives the approximation:

$$\frac{\partial C}{\partial x} \approx \frac{C_{i\pm1} - C_i}{\pm\delta x} = \frac{C_{i+1} - C_i}{\delta x} = \frac{C_i - C_{i-1}}{\delta x}\,. \tag{2.3}$$

To estimate the second derivative, the difference in the last two parts of the equation is divided by δx:

$$\frac{\partial^2 C}{\partial x^2} \approx \frac{(C_{i+1} - C_i) - (C_i - C_{i-1})}{\delta x^2}\,. \tag{2.4}$$

Now Fick's second law of diffusion must be introduced, which describes the change in concentration over time relating to the second derivative of the concentration gradient. This states that spatial differences in concentration will smooth out—a peak in concentration has a negative curvature, and so $\frac{\partial C}{\partial t}$ is negative, meaning that the concentration will decrease. Likewise, a local minima in concentration would experience an increase. This process is dependent on D, the diffusion coefficient:

$$\frac{\partial C}{\partial t} = D\frac{\partial^2 C}{\partial x^2}\,. \tag{2.5}$$

Combining Fick's second law with 2.4 gives:

$$\frac{\partial C}{\partial t} \approx D\frac{(C_{i+1} - C_i) - (C_i - C_{i-1})}{\delta x^2}\,. \tag{2.6}$$

$\frac{\partial C}{\partial t}$ can also be approximated by taking the difference of C at times n and $n+1$ and dividing by a time interval δt:

$$\frac{\partial C}{\partial t} \approx \frac{C(i, n+1) - C(i, n)}{\delta t}\,. \tag{2.7}$$

An approximation for $C(i, n+1)$ is produced by combining 2.6 and 2.7, and solving:

$$C(i, n+1) \approx \frac{D\delta t}{\delta x^2}\left[C(i+1, n) + C(i-1, n) - 2C(i, n)\right] + C(i, n) \tag{2.8}$$

$$C(i,n+1) \approx \frac{D\delta t}{\delta x^2} C(i+1,n) + \frac{D\delta t}{\delta x^2} C(i-1,n) + (1-2\frac{D\delta t}{\delta x^2}) C(i,n) \,. \tag{2.9}$$

Then, substituting with the unit-less factor $\lambda = \frac{D\delta t}{\delta x^2}$:

$$C(i,n+1) \approx \lambda C(i+1,n) + [1-2\lambda] C(i,n) + \lambda C(i-1,n) \,. \tag{2.10}$$

The approximation shown above describes the change in $C(x,t)$ at each time interval n to $n+1$: $C(i,n)$ will decrease in concentration by a factor of $(1-2\lambda)$. Mass is conserved as half of this decrease will be gained by each neighbor $C(i+1,n)$ and $C(i-1,n)$. This is equivalent to a point-wise convolution, with the factor λ representing the kernel. Extending the equation symmetrically to the y axis, this is can be applied to a background-subtracted and bleach-corrected fluorescence image, simulating a step where each pixel diffuses in a one-pixel radius.

At each D over a chosen range, FRAPEvolve convolves a photo-bleached image with the number of time steps to reach the (partially) recovered image. It records how well the images match for each simulated D, and the closest fit at a certain D is the D returned by the program[2].

While powerful in its own right, the FRAPEvolve program is less than robust. The final FRAP image needs to show intensity recovery, but with a diffuse photobleached region still apparent. It also cannot accurately measure a population of more than one diffusion rate. And with an image *too* recovered, the program has no way to accurately match the data, as FRAP images of a fluid bilayer tend towards homogeneity at later time points, losing too much of the image contrast due to diffusion. Another disadvantage is the program's bias in the x and y dimensions, which arise in the evolved image. This is because the simulated diffusion occurs between the four adjacent neighbors of each pixel, with no effect from the four pixels at the diagonals. A better simulation would use a larger pixel radius to produce a more radial convolution, like a Gaussian blur.

2.3.3 Determination of diffusion coefficient by fluorescence correlation spectroscopy

Fluidity can furthermore be determined at the sub-micron scale using fluorescence correlation spectroscopy (FCS), which is a technique to analyze the intensity fluctuations of fluorescent particles using time-dependent autocorrelation (see figure 2.7). Fluctuations in fluorescence intensity can arise from photochemical processes such as triplet state dynamics, photon anti-bunching, and diffusion (both rotational and translational) [51]. Luckily, translational diffusion is the slowest of the fluctuations, occurring on the scale of milliseconds and seconds as a result of fluorescent molecules diffusing into and out of the excitation volume. The autocorrelation

[2]The program also considers the contribution of noise, which facet is not addressed here.

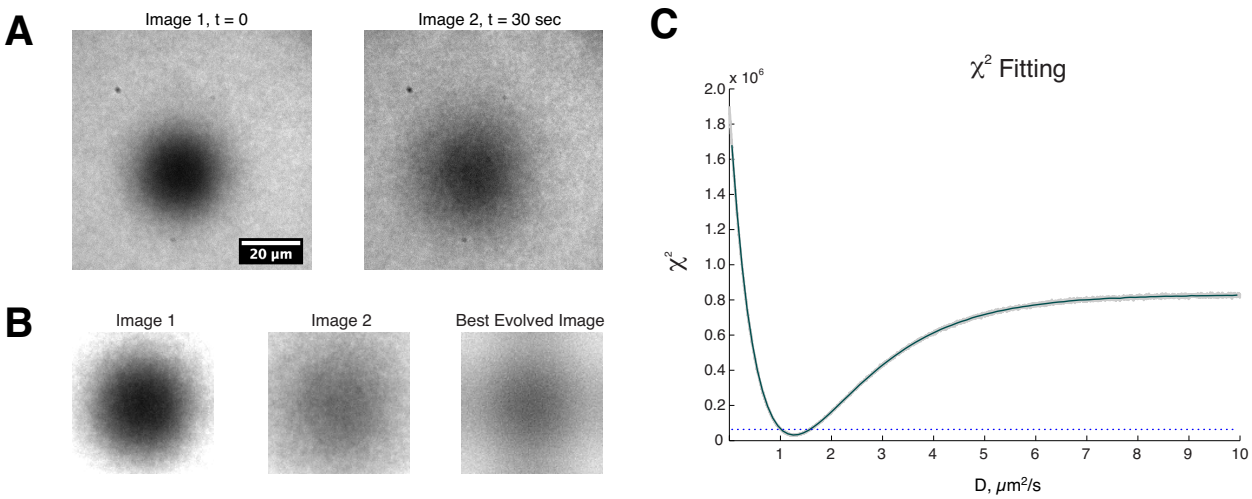

Figure 2.6 – Calculating the 2-dimensional diffusion coefficient from FRAP images. In **A**, 568-Ecad-H12 on a fluid 4% Ni-NTA-DOGS, DOPC bilayer is photo-bleached, with Image 1 taken immediately afterwards, and a partially-recovered Image 2 taken 30 seconds later. **B** shows the cropped regions of Image 1 and 2 that were furthermore background-subtracted, corrected for photobleaching, and rescaled with a pixel bin size of 2. These processed images were used to compare the simulated pixel-wise convolution of Image 1 over a range of D, 0 – 10 μm^2/s. The best evolved image has the minimum χ^2 fit, and corresponds to a D of 1.25 μm^2/s. **C** shows the χ^2 over the range of D, with the intersection of the dotted line corresponding to the interval 0.95 – 1.65 μm^2/s, which results from a σ_D of 0.35 μm^2/s

decay time is largely determined by translational movement, and so the diffusion coefficient of the fluorescent molecules can be extracted from it.

This autocorrelation curve comes from the degree self-similarity of the intensity trace $F(t)$, over a lag time τ:

$$G(\tau) = \frac{\langle \delta F(t) \delta F(t+\tau) \rangle}{\langle F(t) \rangle^2} \tag{2.11}$$

with $\delta F(t) = F(t) - \langle F(t) \rangle$ and the brackets, $\langle \quad \rangle$, denoting the average over all time t. The denominator $\langle F(t) \rangle^2$ is like a normalization factor. The curve for single component 2D diffusion can be fit to the equation

$$G(\tau) = \frac{1}{N} \left(\frac{1}{1 + (\tau / \tau_D)} \right), \tag{2.12}$$

where τ_D is the midpoint of the curve's decay, and N is the average number of fluorescent particles in the illumination spot. Both variables are used to find the diffusion coefficient.

Two differences with FRAP measurements of fluidity are immediate: The first is that FRAP measures fluidity over a scale of several microns, while FCS involves an illuminated area of

$\sim 0.14\,\mu m^2$ created by a diffraction-limited laser spot [52]. The second difference is that FRAP can handle images of a much higher intensity than FCS. Since the goal of an FCS measurement is to capture fluctuation, having too high of a fluorescence intensity can crowd out the fluctuations and make the measurement less sensitive. This can result from either a high density of fluorescent particles on the bilayer or a high excitation intensity. Another drawback of FCS is that capturing the fluorescence fluctuations requires that the excitation occurs at one spot over a certain length of time, and that a wide majority of molecules move out of the illumination volume before photobleaching occurs. Because of this, molecules with a small diffusion coefficient cannot be measured accurately by FCS due to the degree of photobleaching [52].

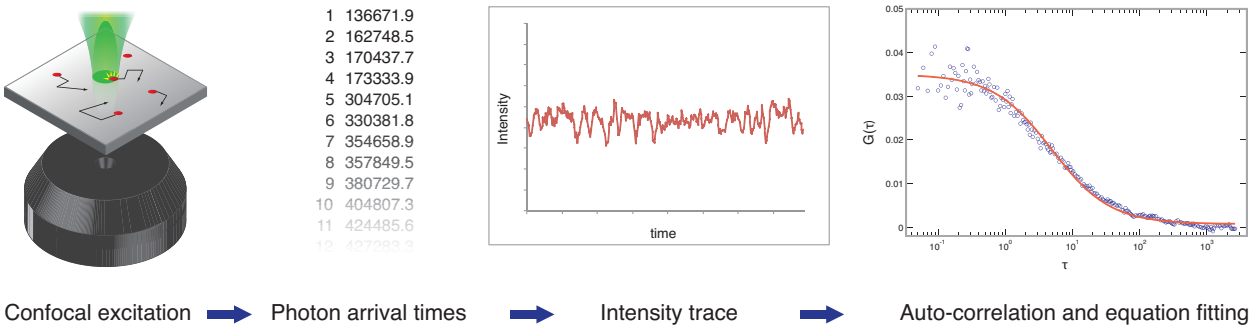

Figure 2.7 – FCS data from a bilayer. Fluorescent molecules diffusing on a bilayer give rise to fluorescent fluctuations in a confocal excitation volume. These are initially recorded at avalanche photodiodes as the arrival times of single photons. Binning the times together produces an intensity trace, which is subsequently autocorrelated with respect to time. The function for single component 2D diffusion is then fit to the data.

The small excitation volume of FCS enables a greater degree of intensity fluctuations to be captured. However, the small size creates challenges in accurately focusing the illumination spot. This spot must be positioned within 100 nm of the bilayer surface, otherwise, having an out-of-focus excitation leads to optical artifacts [52]. On the other hand, finding the position of greatest intensity is not reliable, as the minimum beam waist does not necessarily imply highest intensity count rate [53]. In order to precisely calibrate the surface density with the control bilayer, data from both the sample and control needs to be taken from the minimum beam waist, which is otherwise known as the diffraction-limited minimum size of the beam. This beam size is understood from the equation describing x-y spatial resolution:

$$R_{xy} = \frac{1.22\lambda}{\mathrm{NA}_{\mathrm{condenser}} + \mathrm{NA}_{\mathrm{objective}}}, \tag{2.13}$$

where $\mathrm{NA}_{\mathrm{condenser}}$ and $\mathrm{NA}_{\mathrm{objective}}$ are the numerical apertures of the condenser and objective, respectively. With an epifluorescence microscope, the objective also works as the condenser, and so,

$$R_{xy} = \frac{0.61\lambda}{\mathrm{NA}_{\mathrm{objective}}}. \tag{2.14}$$

With the λ = 568 nm laser and NA = 1.49 objective that were used, this gives a value of R_{xy} = 232 nm. Since the light source is coherent (from a laser), R_{xy} can be slightly smaller [54]. Previous calibrations with TR-DHPE bilayer standards have shown it to be about 210 nm in radius. Thus, a perfectly-focused diffraction limited spot would be a circle with a diameter of ~0.4 μm .

However, using the CCD image to focus the spot to this minimal size is not sufficiently accurate. To overcome this challenge is z-scan FCS, which involves recording FCS data over a range of 50 – 100 nm intervals in height, and graphing the N and τ_D of each position versus z [55]. As the intervals can be known precisely from the piezo-controlled stage with auto-focusing capability, the absolute z value can be floated. Then the N and τ_D of the sample can simply be extrapolated from the minimum y of the fitted parabola, as illustrated in figure 2.8. Similarly, the data can be plotted against z^2 and fit with a linear regression.

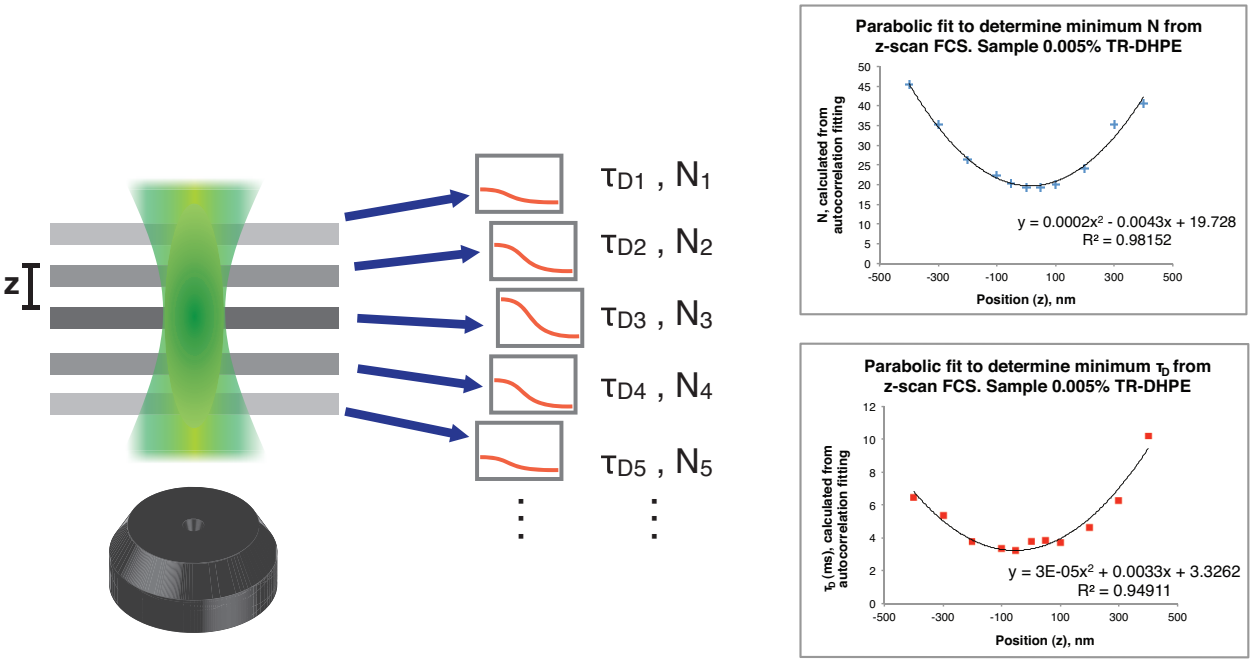

Figure 2.8 – FCS z-scan of control bilayer. Intensity fluctuations are recorded at each z, which intervals are known precisely from the piezo-controlled stage. Then, each z position has an associated autocorrelation curve, from which τ_D and N are determined by fitting the 2D diffusion autocorrelation function. Next, t_D and N are plotted vs. z and fit with a parabola. The value from the theoretical minimal beam waist is extracted from the parabola minimum. In this example, N = 19.7 and τ_D = 3.33 ms.

The spot size is still an important variable but should not change significantly if a system is accurately aligned and focused. To check its value, TR-DHPE calibration bilayers are mea-

sured with z-scan FCS on the same day and with the same settings as the 568-Ecad-H12 bilayer samples. Each calibration bilayer will produce an N from the autocorrelation equation fit with z-scanning, and if the spot size is appropriately focused to its 0.21 μm radius, the density obtained from dividing N by the spot area should match the density expected from the TR-DHPE concentration. This is shown in figure 2.9, which confirms that 0.21 μm can be used as the spot radius for that experiment. With the spot size validated, the relation $D = \frac{\omega^2}{4\tau_D}$ is used to find

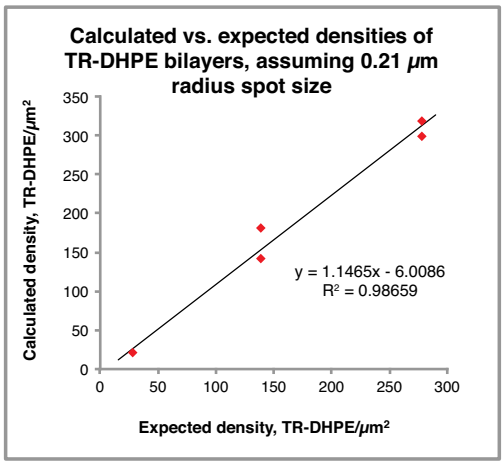

Figure 2.9 – FCS spot size calibration with TR-DHPE bilayers. Three DOPC calibration bilayers doped with 0.001, 0.005, or 0.01 mole % TR-DHPE were measured with z-scan FCS to find N and the corresponding density, assuming a spot radius of 0.21 μm. The plot shows that this assumption is sufficiently accurate for finding 568-Ecad-H12 densities. The 0.001 and 0.005% samples were measured at two locations on the bilayer, and the densities plotted are of TR-DHPE in *both* leaflets of the bilayer.

the diffusion coefficient of the 568-Ecad-H12 with the τ_D produced from the z-scan. This works since τ_D is not only the half-life of the autocorrelation curve decay, but also the average amount of time that fluorescent particles translate within the illumination spot. Thus, it can be used to find their amount of diffusion.

In these experiments, the diffusion coefficient of 568-Ecad-H12 on a 4% NTA-DOGS, 96% DOPC bilayer was found to be $1.6 \pm 0.2\,\mu\text{m}^2/\text{s}$, and FCS data at the minimum beam waist is shown in figure 2.10. This data, and the spot size calibration data, were collected from bilayer samples on an Eclipse Ti inverted microscope (Nikon, Tokyo, Japan). The samples were illuminated by a 5 ps pulsed 568 nm laser (SuperK Extreme, NKT Photonics, Birkerød, Denmark) through a 100 × oil TIRF objective, and emitted photon arrival times were detected with a resolution of 32 ps by single photon avalanche photodiodes (MPD, Bolzano, Italy) and a PicoHarp 300 photon counting module (PicoQuant, Berlin, Germany). To find the intensity fluctuations, the photon arrivals were binned into 10 μs intervals. Matlab scripts (MathWorks, Natick, MA) were used to compute the autocorrelation curve and fit with $G(\tau)$.

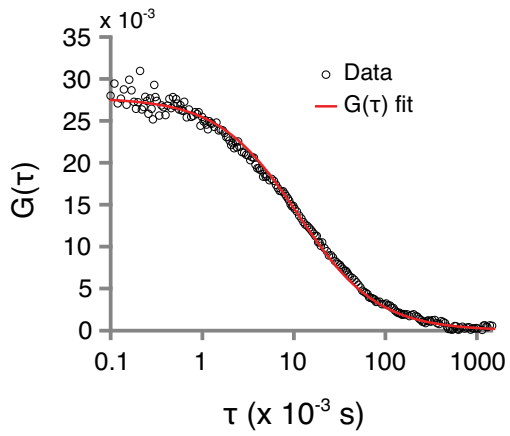

Figure 2.10 – FCS of the 568-Ecad-H12 bilayer. Example FCS curve with fit autocorrelation function is shown. From the data set of z-scan FCS at multiple bilayer positions, 568-Ecad-H12 was determined to have a D of 1.6 ± 0.2 μm^2/s and a density of 320 ± 212 μm^{-2}.

Table 2.3 – 568-Ecad-H12 diffusion coefficients from the three methods mentioned. These values are typical for bilayer-bound proteins.

Method	**Diffusion coefficient, μm^2/s**
Soumpasis's approximation from FRAP	0.7 – 1.1
FRAPEvolve program	1.25 ± 0.35
FCS	1.6 ± 0.2

2.4 E-cadherin density on the bilayer is similar to that on cells

As a means of forming a hybrid cell-cell junction, the surface density is important for creating favorable initial conditions, and some cell-bilayer systems show thresholds of signaling with specific densities [56]. For a free, unrestricted bilayer, diffusion can expose a cell to a greater number of ligands than a cell resting inside or across lipid diffusion barriers. In that case, it would seem that the ligand density of a free, unrestricted bilayer would be a of little consequence. Nevertheless, in our experiments we have checked the surface density of 568-Ecad-H12 to insure that the initial density exposed to the cell is within the range of natural E-cadherin surface densities on cells. Duguay et al. report a cell to contain 2.5×10^4 – 16×10^4 E-cadherin molecules on its surface [57]. Assuming a cell's surface area to be that of spheres between 10 and 15 μm diameter, this gives a range of 314 – 707 E-cadherin/μm^2. As the following data of bilayer measurements show, the density of 568-Ecad-H12 can be successfully matched within this physiological range.

Interestingly, however, is that the diffusive nature of an unrestricted bilayer allows for an

essentially unlimited number of bilayer E-cadherin to access areas of cell binding where bound E-cadherin molecules are in a diffusion trap of little to no mobility [16]. The diffusion into cell contacts is apparent in images such as figure 3.2 on page 37. Thus, bilayer densities below physiological range may not provide any difference in cell binding behavior, but in some cell-bilayer-ligand systems, densities show an effect and can trigger different cell signaling events [56].

2.4.1 Quantitative fluorescence

Determining density by quantitative fluorescence involves calculating the ratio of a lipid probe's brightness on a bilayer and in solution (within vesicles), and comparing that ratio, times a scaling factor, to the protein's brightness in solution, in order to find the unknown protein density on the bilayer. This technique uses the optical-train measurement method discussed in Galush et al., meaning that the calibration is specific for the microscope and filter set used [58]. Quantitative fluorescence was employed to calibrate the intensities within figures 3.2 and 3.5.

To begin, a fluorescent lipid probe must be chosen that can be imaged with the same filter cube or filter set as the protein of interest. In the case of 568-Ecad-H12, Texas Red-DHPE was used. Lipid vesicles are made with a range of lipid probe concentrations, or otherwise diluted in buffer. Epi fluorescence images are taken on the microscope of the vesicle solutions, with the focal plane in solution and the same acquisition settings for each sample. The same is done with a titration of the protein, using the same acquisition settings and z-position. As the purpose is to measure the fluorescence intensity within the solutions, an objective with a lower NA yet higher working distance is used. Including a blank measurement, these data are plotted as intensity versus molar concentration, as in fig 2.11. The slopes of these values are $I_{\text{probe(solution)}}$ for the lipid probe and $I_{\text{sample(solution)}}$ for the protein of interest. The ratio of these provides a scaling factor, F, which relates the molar brightness of the protein sample and the lipid probe:

$$\frac{I_{\text{sample(solution)}}}{I_{\text{probe(solution)}}} = F\,. \tag{2.15}$$

Here, a calibration curve, similar to the previous solution measurements, is constructed from intensity measurements from a range of lipid probe bilayer concentrations, including a blank. These bilayer measurements require the same filter set and microscope from the solution measurements, but a higher NA objective may be swapped. Instead of graphing molar concentration on the x-axis, density takes its place. Using the knowledge that a DOPC lipid head group in a bilayer occupies a space of 0.72 nm^2 (equivalently speaking, 1 μm^2 of a bilayer contains 1,388,889 DOPC molecules in a single leaflet) [59], the density of the lipid probe can be calculated based on its molar ratio. Graphing the probe intensity versus density produces the slope $I_{\text{probe(bilayer)}}$. Since $I_{\text{probe(bilayer)}}$ is a measure of molar brightness, the scaling factor is used again, except with bilayers:

$$\frac{I_{\text{sample(bilayer)}}}{I_{\text{probe(bilayer)}}} = F\,. \tag{2.16}$$

With the calculated $I_{\text{sample(bilayer)}}$, the background-substracted intensity is measured from the protein bilayer, and the density is back-calculated. If the sample protein is attached to one leaflet of the bilayer, unlike the lipid probe, which is in both leaflets, a factor of 2 must be used:

$$\text{protein density} = 2 \times \frac{\text{intensity}}{I_{\text{sample(bilayer)}}}\,. \tag{2.17}$$

Though it goes without saying, this is only a measurement of actively fluorescent protein on the bilayer, rather than all the protein attached. A fluorescent fusion protein sample may contain a significant population of proteins in a dark state that still retains biological function. Similarly, proteins that are chemically labeled may have different extents of labeling.

The advantages of quantitative fluorescence is that protein density can be measured in dense cell contacts, such as in figure3.2, and on non-fluid surfaces, using a simple comparison to calibration bilayers and a blank. Additionally, once the scaling factor is determined for a particular microscope and filter set, the number can be used for future experiments. The disadvantage of the technique is that it relies on the assumption that the fluorophore brightness does not change between the bilayer and solution measurements. Depending on the nature of the fluorophore and the protein, this may or may not be a significant effect. Likewise, the linearity between fluorophore intensity and surface density is lost above 0.5 mole %, due to self-quenching and FRET effects [58].

Another disadvantage is that the calibration curve of the protein in solution relies on knowing the concentration of fluorescently active protein in the sample. In practice, because the sample has a small total volume and is not very concentrated, a Thermo-Fisher Nanodrop spectrophotometer is used because it can take measurements with only 1 – 2 μL of sample. The concentration fluorescently active protein is calculated by dividing the absorption at the fluorescence excitation wavelength by the fluorophore's molar extinction coefficient. However, this absorption measurement is often weak and not robust for a typical ~1 – 10 μM (~0.1 – 1 mg/mL) fluorescent protein sample.

2.4.2 Fluorescence correlation spectroscopy

As mentioned earlier in section 2.3.3 on page 22 , the correlation curve can be fit to an equation to yield N, the average number of particles in the illumination spot, which can then be compared against a calibration bilayer to calculate the sample's 568-Ecad-H12 density. From the FCS data, this density turns out to be 320 ± 212 μm^{-2}. Since FCS is accurate for low surface densities, this can be a reliable technique for bilayers of a weak intensity.

The drawback, as mentioned earlier, is that non-fluid or low-fluidity surfaces cannot be measured due to a lack of fluctuations. Similarly, bilayers with a high intensity cannot be accurately measured for the same reason. Also, the N acquired from FCS is the average number of

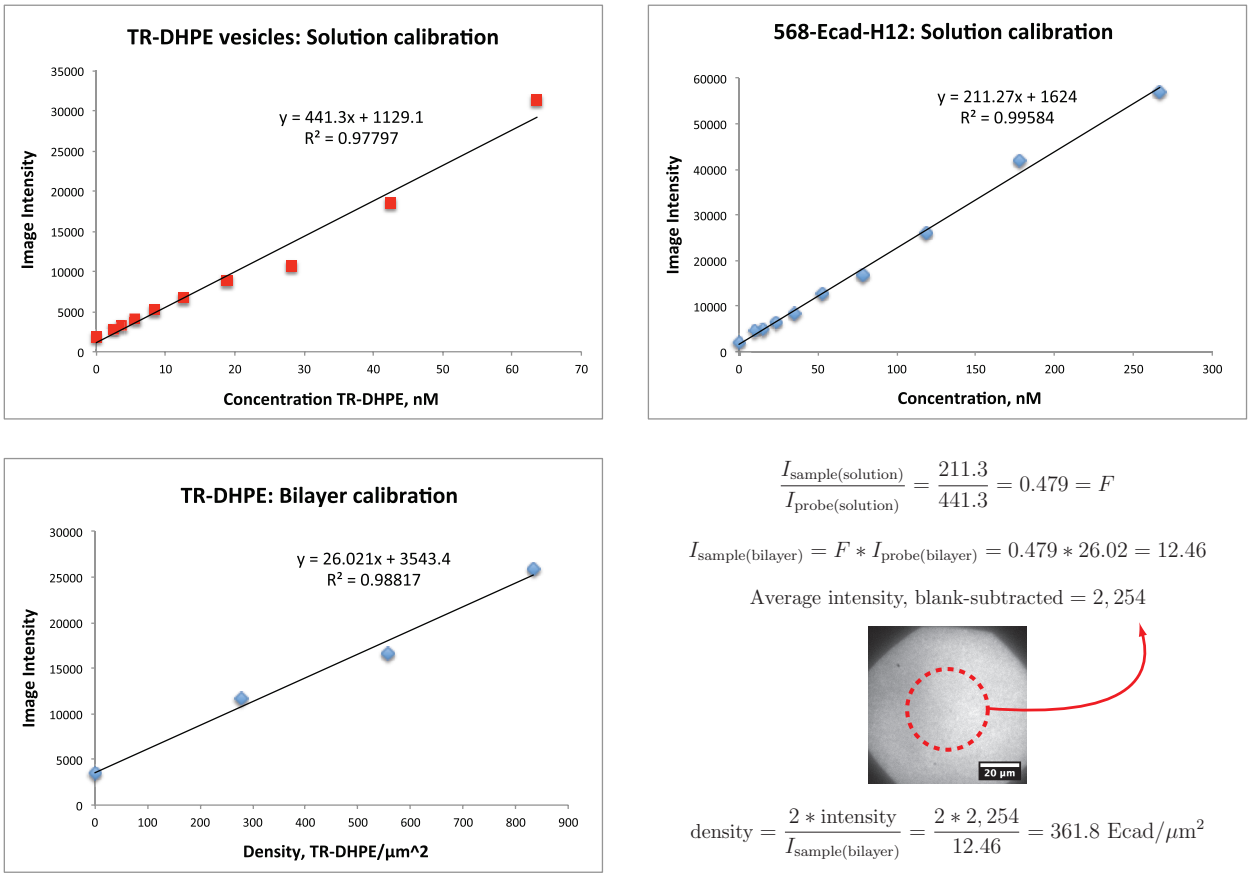

Figure 2.11 – Example of quantitative fluorescence calculations. The scaling factor F is determined from the ratio of slopes from solution calibrations. This factor is applied to the slope of the Texas Red bilayer calibration to find the relation between the protein sample's intensity and its surface density. This relies on the assumption that the intrinsic molecular brightness of the probe and sample do not change between solution and bilayer measurements.

particles—not molecules—and so monomers, dimers, trimers, and so on, would be calculated all as particles, rather than the number of their constituent molecules.

2.5 Photon counting histogram analysis shows E-cadherin to exist on the bilayer as a single oligomer

2.5.1 Limitations of quantitative fluorescence microscopy and FCS in determining oligomerization state

Since N as determined by FCS is the average number of fluorescent *clusters* within the illumination volume, and quantitative fluorescence resolves the number of fluorescent *molecules*,

simply dividing the number of molecules by the number of clusters will produce the average number of molecules per cluster.

However, depending on the fluorophore, quantitative fluorescence may not be as accurate of a technique to fold into the FCS measurement. In the case of the 568-Ecad-H12 construct, the Alexa 568-maleimide fluorophore is located close to the C-terminus of the protein. With the protein linked to a Ni-NTA bilayer, this configuration places the fluorophore in close proximity to the bilayer surface, where fewer water molecules would be able to interfere and quench the fluorescence. Thus, the quantum yield on the bilayer is higher than in solution. The current technique of quantitative fluorescence involves comparing the fluorophore brightness in solution versus on the bilayer, with the assumption that the linking to a bilayer has no effect on the fluorescence properties, as mentioned previously. Of course, the more appropriate bulk solution measurement would be with the protein linked to lipid vesicles, and this would require that all the protein present be attached. Unfortunately there is no practical way to ensure this to a high level of accuracy. Rinsing the buffer would rinse out some portion of vesicles. Using bilayer-coated beads may work, but again one has to know the molar concentration of the bound protein and ensure that it stays put throughout the measurement.

Another straightforward, but limited, technique to determine the oligomerization state is by fitting a two-species autocorrelation equation to the data [60]. However, this requires the two diffusion coefficients to have a large enough difference that the fitting can work [36]. Dimerization may not produce a large enough change, as the diffusion coefficient of membrane-bound molecules is more dependent on the surrounding lipids than the protein's size, with oligomerization playing a non-linear scaling effect [47, 61].

2.5.2 Photon counting histogram

With the limitations of quantitative fluorescence and FCS, the better method of determining oligomerization state is to analyze the fluorescence fluctuation data with a photon counting histogram, and compare this to a fluorescence lipid probe control assumed to diffuse as 100% monomers. This type of analysis was used with 568-Ecad-H12 and Texas Red-DHPE to find that 568-Ecad-H12 exists as a single oligomer while attached to a fluid bilayer.

The photon counting histogram (PCH) is simply a binning of photon arrival times from the intensity trace used in the autocorrelation. A bin size smaller than the molecule dwell time is chosen so that the counting relates to molecule cluster size but not the degree of mobility. With that, the intensity trace leads to a super-Poisson distribution of photon counts [62]. By fitting the appropriate equation for the Poisson distribution of multiple diffusing species, the molecular brightness, ϵ, and number of species within a chosen volume can be determined. The equations behind the PCH can be understood by starting with a single stationary fluorophore, and then allowing for the effects of illumination, movement, and multiple particles on the counting statistics.

For a single immobile fluorescent particle, the distribution of its emitted photons can be described by a Poisson distribution:

$$\mathrm{Poi}(k;\langle k\rangle) = \frac{\langle k\rangle^k}{k!} e^{-\langle k\rangle} \tag{2.18}$$

Here, k is the number of photons reaching the detector ("counts") in a fixed time period, and $\langle k\rangle$ is the average number of arrivals in that period. The Poisson distribution gives the probability that k photons will arrive. In other words, $p(k) = \mathrm{Poi}(k;\langle k\rangle)$. Additionally, for pure Poisson behavior, $\langle \Delta k^2\rangle = \langle k\rangle$.

However, in the case of fluorescence there are two fluctuating streams of photons to consider: first, the excitation photons from the light source, and second, the emission photons from the fluorophore. The combination of these two variables leads to a super-Poisson distribution, meaning that $\langle \Delta k^2\rangle > \langle k\rangle$. This makes the PCH broader than if it was representing a true Poisson distribution. Fortunately, the difference is not huge given the fact that the two fluctuating streams of photons follow each other: a burst of excitation photons proportionally leads to a burst of emitted photons. As long as a small time interval is chosen—so as not to average out the fluctuations—the PCH of the fluorescent particle is roughly Poissonian.

The emission of photons furthermore depends on the point spread function (PSF), which is the measured fluorescence intensity of a particle at a position r. The intensity at the detector for one-photon excitation is:

$$I_D(r) = I_{ex}\,\beta\,\mathrm{PSF}(r). \tag{2.19}$$

Where I_{ex} is the excitation intensity at the center of the PSF and β is a scaling factor dependent on excitation probability, quantum yield, and optical characteristics of the instrument. The molecular brightness, ϵ, is the average number of counts per second per molecule (cpsm), and is related by $\epsilon = I_{ex}\,\beta\,\eta$, with η being a measure of detection efficiency.

Now, for the single immobile particle at a position r_0, $\langle k\rangle$ is taken as $\epsilon\mathrm{PSF}(r)$ so that the PCH is

$$p(k;r_0,\epsilon) = \mathrm{Poi}(k,\epsilon\mathrm{PSF}(r_0)). \tag{2.20}$$

Now, the particle is allowed to diffuse within a volume V_0 inside the PSF. The probability that the particle is at a position r is $p(r)$. Then, the PCH becomes

$$p(k;V_0,\epsilon) = \int \mathrm{Poi}(k;\epsilon\mathrm{PSF}(r))\,p(r)\,dr. \tag{2.21}$$

This is the average of the Poisson distributions for the particle at every location in V_0, each weighted according to the PSF's influence on molecular brightness. If the single particle moves to all parts of V_0 with equal probability, then $\int p(r)\,dr = \frac{1}{V_0}$, and so

$$p^{(1)}(k;V_0,\epsilon) = \frac{1}{V_0}\int_{V_0} \mathrm{Poi}(k;\epsilon\mathrm{PSF}(r))\,dr. \tag{2.22}$$

For a PCH of two identical particles acting independently of each other, the combined distribution, $p^{(1+2)}$, is the sum of the Poisson distributions for all possible positions of the second particle, at each possible position of the first particle:

$$p^{(1+2)}(k;V_0,\epsilon) = \sum_{r=0}^{k} p^{(1)}(k-r)\,p^{(2)}(r). \tag{2.23}$$

This can be expressed as a convolution of the two distributions, and is easily extended to accommodate N identical particles:

$$p^{(N)}(k;V_0,\epsilon) = p_1^{(1)} \otimes \ldots \otimes p_N^{(1)}. \tag{2.24}$$

For a second species of a different brightness, acting independently of the first species, there will be N_1 particles in the volume with molecular brightness ϵ_1, and N_2 particles with ϵ_2. The PCH of the two species system is given by another convolution:

$$p^{(N_1,N_2)}(k;V_0,\epsilon_1,\epsilon_2) = p_1^{(N_1)}(k;V_0,\epsilon_1) \otimes p_1^{(N_2)}(k;V_0,\epsilon_2). \tag{2.25}$$

The Globals software package (developed at the Laboratory for Fluorescence Dynamics at the University of Illinois at Urbana-Champaign) was used to fit a two-species PCH from equation 2.25 to the intensity fluctuation data to extract N_1, ϵ_1, N_2, and ϵ_2, (figure 2.12), using a 2D Gaussian point spread function. If the protein forms dimers or higher-order oligomers, the molecular brightness will increase by two or more times.

By fitting the two-species PCH to the data, it was determined that $\epsilon_1 = \epsilon_2$, which is equivalent to saying that there is only one oligomeric species. Most likely, this is a monomer, given the homogeneous fluidity of the protein. Proteins that cluster on the bilayer tend to form aggregates that are visible with epifluorescence imaging. Also, if the species on the bilayer was a dimer, the single oligomer characteristic means it would have to be 100% dimer. As the protein has been shown to be monomeric in solution, it would be unreasonable to expect it to completely dimerize with no trace of a monomeric population. The most rigorous experiment to prove the dimerization state of the protein would be to use, as a control, the 568-Ecad-H12 construct in which the residues causing cis-affinity, V81 and L175, are mutated to aspartic acid. In this case the molecular brightness of the cis-mutant could be taken as the molecular brightness to expect of monomeric 568-Ecad-H12.

2.6 Summary of E-cadherin bilayer characterization

A protein construct consisting of the E-cadherin extra-cellular domain, a site-specific fluorophore, and a histidine motif was chosen based on its ability to create fluid, homogeneous

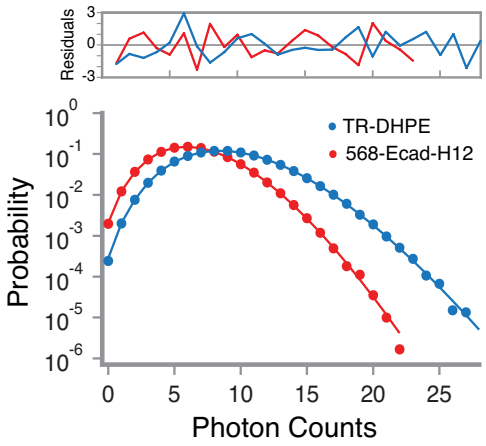

Figure 2.12 – Photon counting histogram of 568-Ecad-H12 bound to a fluid DOPC bilayer. Here, a PCH was generated by binning emitted photon arrivals of a 568-Ecad-H12 bilayer (2% NTA-DOGS, 98% DOPC) into 200 μs time intervals and normalizing over the total photon counts. Assuming a two-dimensional Gaussian PSF, the Globals program was used to fit a super-Poisson distribution for multiple diffusion particles of two species with molecular brightness ϵ_1 and ϵ_2. The program calculated that the two species have a brightness $\epsilon_1 = \epsilon_2 = 2,022$ cpsm. As the two species have equal brightness, it follows that the 568-Ecad-H12 is present as a single oligomer. A control bilayer sample of TR-DHPE, which is known to be monomeric, was used to check that the Gaussian PSF fit.

protein bilayers, and elucidate a cell response that includes adhesion and enrichment of protein surface density. This construct, 568-Ecad-H12, was attached to bilayers of 4% Ni-NTA-DOGS and 96% DOPC by Ni^{2+}-histidine chelation. FRAP and z-scan FCS confirmed protein fluidity; more specifically, FRAP showed fluid coverage over an area of microns, and z-scan FCS confirmed protein fluidity at a sub-micron level. Both methods were used to measure the diffusion coefficient of the protein. The surface density of the protein was determined by z-scan FCS and quantitative fluorescence measurements, and this value was comparable to the density of E-cadherin on the cell surface. PCH analysis of the intensity trace confirmed that the protein exists in a single oligomeric state on the bilayer, which is likely a monomer.

Chapter 3

Cell adhesion to the E-cadherin lipid bilayer

In conjunction with the physical characterization of E-cadherin on the bilayer, the biological relevance of this synthetic membrane was examined by culturing live cells on its surface. Of the multiple E-cadherin constructs that were tested, it was the 568-Ecad-H12 construct that was first to demonstrate both fluidity *and* a positive cell interaction of E-cadherin enrichment with the human gastric cancer cell line MKN28. Thus, the 568-Ecad-H12 bilayer was examined further with MKN28 cells, exposing interesting properties of E-cadherin adhesion that will be discussed in this section.

3.1 Cell attachment analysis on protein-coated glass

To test if the purified 568-Ecad-H12 was biologically active (able to support favorable binding with cells), the protein, and three other proteins as controls were each adsorbed to a 25 mm diameter glass coverslip, and the attachment of seeded cells was monitored. The three control proteins used were BSA, 647-Goat anti-rabbit secondary antibody (Life Technologies), and E-cadherin-Fc (R&D Systems, Minneapolis, MN). The secondary antibody was chosen as a control against the Fc region, which is also present in the E-cadherin-Fc. Each protein was diluted to a concentration of 1.5 μg in 40 μL TBS+Ca, and placed as a drop in a plastic petri dish. Then, a UV-treated, dry, hydrophilic glass coverslip was placed on top each drop, in order to evenly spread the protein solution across the glass surface. These assemblies were allowed to incubate for 2 hours at room temperature. Then the coverslips were assembled into Attofluor Cell Chambers (Life Technologies), which were rinsed with TBS+Ca and then replaced with RPMI culture media, supplemented with 10% FBS and 1% penicillin and streptomycin solution.

MKN28 cells were dissociated from culture dishes with 0.05% trypsin-EDTA solution and were added for a total of 1.2 $\times$ 10^6 cells in each chamber. After a 4 hour incubation period, the chambers were rinsed rigorously with 10 mL TBS+Ca by aiming the pipette's outflow at the coverslip. Then 5 transmitted light images were taken at random, but central, locations of each sample, using an inverted microscope and a 40 $\times$ air objective. Only cells in the middle 500 μm $\times$ 500 μm region of each image were counted. The analysis showed that cells were more

likely to stay attached on the E-cadherin-Fc and 568-Ecad-H12 surfaces than on the secondary antibody or BSA. This simple experiment supports the notion that the purified and labeled 568-Ecad-H12 enables cell binding as much as the commercial E-cadherin-Fc, which is routinely used in E-cadherin experiments.

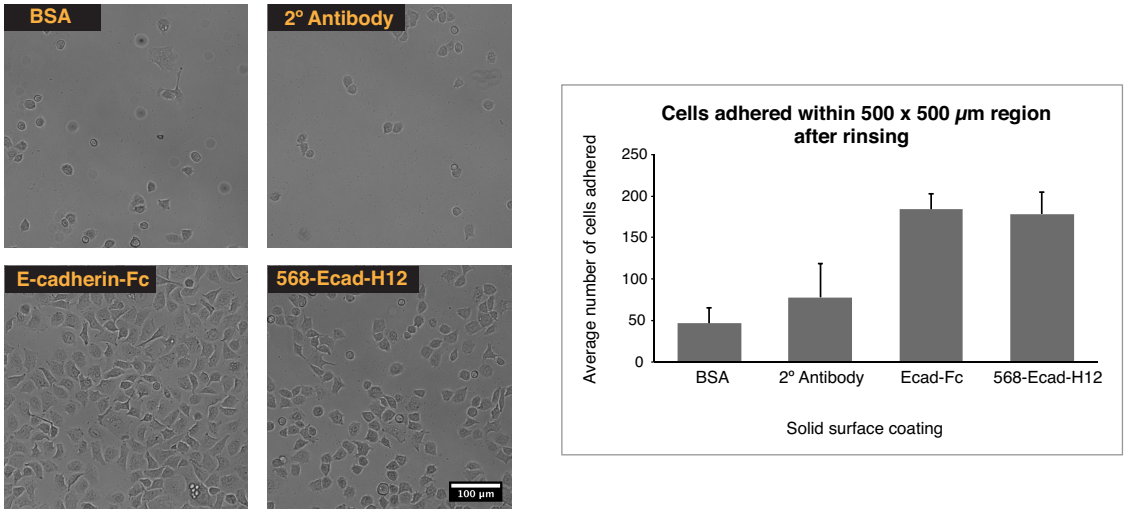

Figure 3.1 – Cell attachment rates on protein-coated glass. Protein solutions of a concentration 1.5 μg in 40 μL each were added to dry, hydrophilic glass coverslips and allowed to incubate 2 hours. These proteins were 568-Ecad-H12, commercial E-cadherin-Fc, BSA, and a secondary antibody (647-goat anti-rabbit IgG). After rinsing and replacing with media, an equal number of MKN28 cells was added to each. After 4 hours of incubation, the coverslips were forcefully rinsed, and the average number of cells in a 500 μm × 500 μm region was determined. Representative images for each are shown. A total of five regions were averaged for each sample, and the numbers with standard deviations are plotted in the graph. The purified and labeled 568-Ecad-H12 supports a similar number of adhering cells as the E-cadherin-Fc. Cells show small amounts of non-specific adhesion to BSA and antibody coated surfaces. The antibody was used as a control against the IgG region of E-cadherin-Fc.

3.2 Fluid DOPC

There are two main physical readouts of interest in identifying cell and bilayer-E-cadherin interactions. These are the tight adhesions highlighted by reflection interference contrast microscopy (RICM), and more importantly, the enrichment of fluorescent bilayer E-cadherin underneath the cell surface. RICM images the reflection of a narrow bandwidth of light. An object with a close interface to a coverslip creates deconstructive interference due to the phase shift in the reflected light. Thus, in cell imaging, the parts of the cell that adhere closely to the coverslip appear dark, which makes RICM a useful imaging mode to confirm cell-substrate binding [63]. The other readout, an accumulation of bilayer-E-cadherin within the cell contact region, is a

sign of the cell's surface proteins binding to the bilayer E-cadherin. This occurs when the cell binds to protein at the initial bilayer density while allowing more bilayer E-cadherin to diffuse into the contact region.

The condition that the bilayer-E-cadherin is actually bound by the cell's E-cadherin (as opposed to other proteins or other cadherins) can be determined by imaging the intercellular domain of the cell's E-cadherin and seeing if it overlaps with the bilayer E-cadherin. This overlap is known as co-localization, and can be imaged by fixing and immunostaining the intercellular domain of E-cadherin. Another technique is to use cells transfected with a fluorescent fusion of E-cadherin, such as mCherry or eGFP. In this case the fluorescent protein domain exists in the intercellular domain, so that the extracellular binding events are relatively unperturbed. However, while the fluorescent transfection of cells provides extensive capabilities such as localizing a cell's protein in real time, the transfection of cells may also cause over-expression of a protein, leading to a bias of certain biological effects.

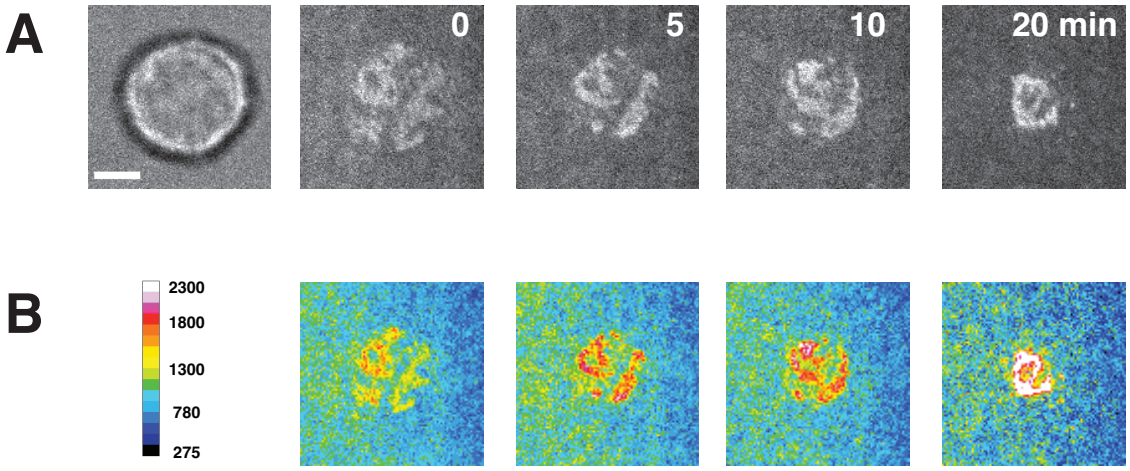

Figure 3.2 – MKN28 on fluid 568-Ecad-H12. Time sequence of cell remodeling a fluid contact of 568-Ecad-H12. Time corresponds to start of movie, which begins 37 minutes after the addition of cells. Row **A** shows original images. Intensity is due to fluorescence of 568-Ecad-H12, except for leftmost image, which is transmitted light. Row **B** shows images that have been rescaled to correct for photobleaching and calibrated to TR bilayer standards. Values on calibration bar denote molecules of 568-Ecad-H12 per μm^2. Scale bar, 5 μm.

As mentioned earlier, the first positive signs of cells interacting with bilayer-linked E-cadherin occurred with MKN28 cells and a DOPC bilayer displaying 568-Ecad-H12. This is a human gastric cancer cell line that expresses E-cadherin and forms tightly-adhering epithelial sheets in culture [64]. The protein bilayer was prepared as in section 2.1.2 on page 14. MKN28 cells were grown in RPMI 1680 media (Invitrogen) with 10% FBS and 1% penicillin/streptomycin in a 37 °C incubator with 5% CO_2.

For the experiment, the cells were detached from culture by incubating with enzyme-free cell dissociation buffer (Hank's based, Life Technologies), and cell aggregates were separated by

gentle pipetting. The dissociation buffer was neutralized with an imaging buffer consisting of 50 mM HEPES, 150 mM NaCl, 5 mM KCl, 1 mM $MgCl_2$, 11.1 mM D-glucose, 2 mM $CaCl_2$, and pH balanced to a pH of 7.4. This imaging buffer contains salts and glucose used at the same concentration as in RPMI, but with extra Ca^{2+}. Cells were concentrated and resuspended in a smaller volume of the imaging buffer, and the sample imaging chamber was also rinsed with the same buffer. The cells were then added to the chamber at a low density, in order to keep single cells from crowding and interacting with each other. The sample chamber was maintained at 37 °C, and E-cadherin binding events occurred anywhere from 40 minutes to 3 hours after introducing the cells. Figure 3.2 gives a time-lapse image sequence of an E-cadherin enrichment event that was typically observed when cells bound to fluid protein.

3.2.1 Frequency of junction formation is low on the DOPC bilayer

However, cell binding with E-cad enrichment occurred at a very low frequency. Only 1% or less of the cells added to the sample chamber formed these types of adhesions; this is the average percentage from eight experiments where at least 50 cells were counted in each. As the cells were known to adhere favorably to glass-adsorbed E-cadherin, methods were sought to decrease the fluidity of the 568-Ecad-H12 bilayer. These methods included nano-patterned diffusion barriers (grids) within a fluid bilayer, using an antibody to force the oligomerization of 568-Ecad-H12, using a low-mobility film of DMPC lipids, and using a gel-phase DPPC bilayer. For each, cells were allowed to react with the protein for 2 – 3 hours. Afterwards, cells were counted, or fixed and then counted, for adhesions showing enriched 568-Ecad-H12 in the contact region. Results are summarized in figure 3.6 on page 43.

3.3 Nanopatterned grid lines

Glass coverslips were patterned with chromium diffusion barriers of 5 nm height, 100 nm width, and pitches of 1 – 4 μm to block lipid mobility. These were created by nano-imprint lithography, which has been discussed in previous publications [42, 65]. This fabrication process involved pressing a silicon-based imprint mold onto cover-slips coated with UV-curable imprint polymers. The polymer coating was cured by UV exposure, and the imprinted patterns were extended to the glass surface by oxygen plasma etching. Next, thermal evaporation was used to deposit a thin layer of chromium over the entire patterned region. The chromium evaporated onto the glass surface remained as the diffusion barrier, and chromium elsewhere on the polymer coating was removed by resist lift-off processing.

These diffusion barriers work by the simple mechanism that fluid lipid bilayers cannot form over their surface. Thus, proteins attached to lipid head-groups cannot be transported across. The restriction of lateral mobility of bilayer-bound receptors has exposed interesting characteristics of spatial organization in cell signaling [33, 66]. In these cases, geometry of the receptors or ligands affects the biochemical signaling within the cell. As these physical barriers limit the cell's active transport of surface proteins, the barriers impose a force against a cell's pulling of

surface attached molecules. So, if the E-cadherin junction formation on a bilayer is triggered by force, bilayer E-cadherin should be clustered along the edges of the diffusion barriers where force can nucleate adhesion. Furthermore, this adhesion event should occur with a greater probability than E-cadherin junction formation on fluid DOPC bilayers.

Remarkably, this use of the diffusion barriers with fluid 568-Ecad-H12 did not increase the rate of E-cadherin junction formation compared with cells on an unrestricted DOPC bilayer. This implies that force implemented on micron-length scales through the use of imprinted nano-patterns is not sufficient for triggering the adhesion formation. Furthermore, of the few adhesions that were observed, cellular E-cadherin did not transport the bilayer 568-Ecad-H12 to the edges of the chromium barriers where such force-dependent strengthening could have taken place. Of the few rare events of 568-Ecad-H12 enrichment on DOPC bilayers, those on nano-patterns, such as figure 3.3, show no difference to the barriers. Across five experiments, an average of only 3% of the cells added showed adhesions with enriched 568-Ecad-H12.

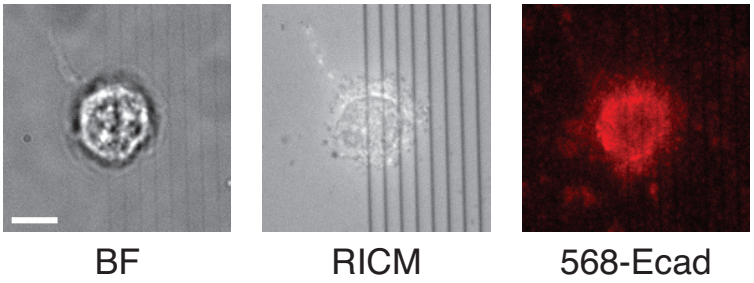

Figure 3.3 – MKN28 forming adhesion on fluid 568-Ecad-H12 with diffusion barriers. Nano-patterned chromium lines of 2 μm restrict lateral transport of the 568-Ecad-H12. However, the protein cluster shows no difference between the restricted and unrestricted halves of the cell adhesion. This suggests that even in the rare events of cells forming E-cadherin adhesion junctions on nano-patterns, the type of resistance imposed by the barriers is unnecessary. Scale bar, 5 μm.

3.4 Forced oligomerization of E-cadherin on the bilayer using antibodies

As 568-Ecad-H12 had been shown to exist in a single oligomeric state on a fluid DOPC bilayer by PCH, an antibody against the polyhistidine on the C-terminus (mouse anti-Histag, Life Technologies) was used to create dimers and higher order oligomers of the protein without perturbing the formation of strand-swapped trans-dimers with cells. In some cases, forcing dimerization of originally monomeric ligands on the bilayer can drive their clustering and transport by the cell [35, 36].

This experiment was done by diluting the antibody to a final concentration of 0.5 μg/mL in the TBS+Ca supernatant of a prepared 568-Ecad-H12 DOPC sample. This was incubated at room temperature for 60 minutes, and then rinsed out with buffer. The fluorescence intensity

of the bilayer-bound protein did not change significantly after the addition of the antibody, suggesting that the antibody did not interfere with the Ni-NTA and his-tag chelation. Also, FCS measurements showed the diffusion coefficient of the 568-Ecad-H12 to be reduced by a factor of four with the antibody addition, from 1.6 to 0.4 $\mu m^2/s$.

However, from counting the cells across three different experiments, only ~1% of the MKN28 cells showed enriched E-cadherin adhesions, demonstrating no improvement over the results obtained with the original DOPC bilayer.

3.5 Low-mobility DMPC surface

To investigate cell binding to a low-fluidity surface, a lipid film was created on a glass coverslip with DMPC lipids doped with 4% Ni-NTA-DOGS. Though a DMPC lipid bilayer has a gel phase transition temperature of 23 °C, the extremely low fluidity of this DMPC lipid film at 37 °C suggests oxidized lipids or lipids adsorbed directly to the glass. Thus, the low-fluidity DMPC cannot be considered a bilayer, but rather a thin film or coating of lipids.

Nevertheless, 568-Ecad-H12 can still be attached to this surface to create a low-mobility display of E-cadherin (figure 3.4). Instead of an entirely non-fluid E-cadherin surface, such as one created by covalent attachment of E-cadherin to the glass coverslip [32], cells are able to laterally transport the E-cadherin bound to the lipid film. This interaction showed 568-Ecad-H12 enrichment by the cell (figure 3.5), but with a different phenotype compared with the highly fluid DOPC surface. The main difference is that the bilayer E-cadherin is only transported from the outside of the cell to the periphery, rather than to the center of the cell adhesion. Most likely, this difference is a direct result of physical surface properties, rather than biochemical changes within the cell. With fluid surfaces, there is the possibility that the cell clusters the 568-Ecad-H12 from the outside, and that this protein is passively pushed inwards by the centripetal flow. There is also the physical effect of the cell's contact area. Cells on solid surfaces such as a culture flask tend to spread. Cells adhering to fluid surfaces tend to contract due to the lack of a counteracting force. Such contraction decreases their contact area on fluid surfaces.

Strikingly, the rate of enriched adhesions was 54% across 4 separate experiments, significantly higher than the other 568-Ecad-H12 lipid surfaces.

3.6 Gel-phase DPPC bilayer

Samples of 568-Ecad-H12 on DPPC bilayers were formed just as with DOPC, but with replacing one lipid species with the other. While some protocols recommend forming DPPC bilayers with all buffers above the gel phase transition temperature of 41 °C, it was found through FRAP analysis that DPPC bilayers formed at room temperature show homogeneous surfaces (by fluorescent lipid probe), and appropriate phase transition upon gentle warming. This suggests that forming DPPC bilayers at room temperature poses no serious risk.

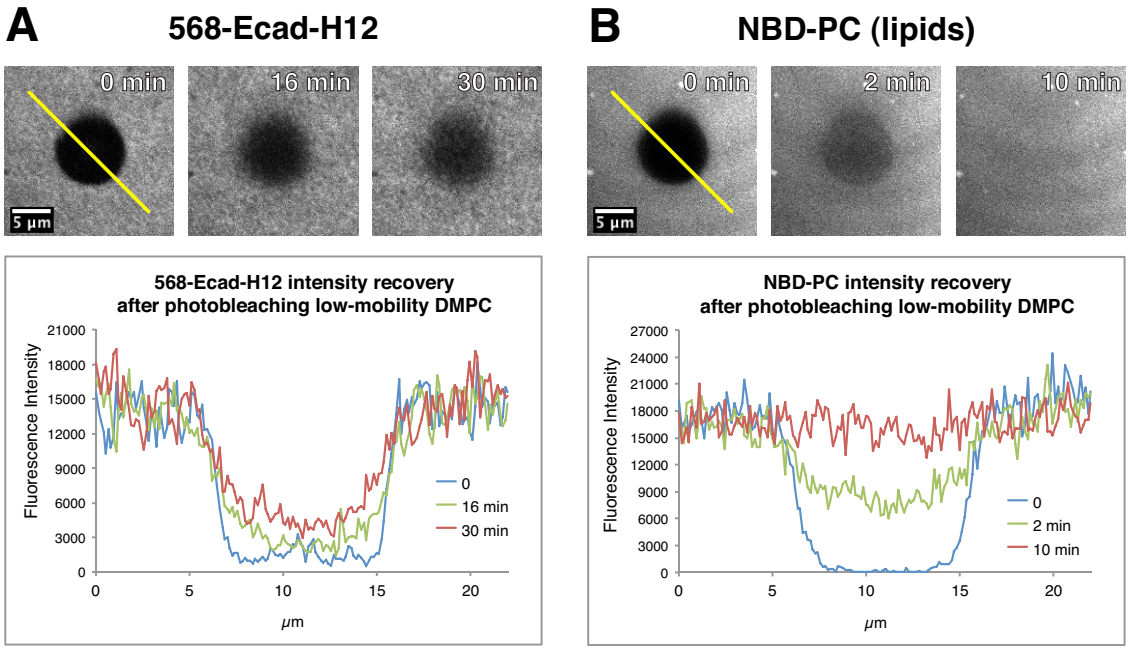

Figure 3.4 – FRAP of low-mobility DMPC surface. A bilayer was prepared with 95.9% DMPC, 4% Ni-NTA-DOGS, and 0.1% NBD-PC, and incubated with 568-Ecad-H12 according to the protocol previously mentioned. However, the protein-lipid bilayer resulted with slower diffusive properties than would be considered normal for a DMPC bilayer at 37°C. **A** shows the photo-bleached 568-Ecad-H12 and line scan through the center. There is a slight intensity recovery at the edges. **B** shows the same region of the bilayer, which was photo-bleached and monitored simultaneously as the data in **A**. Images and line scan show that NBD-PC recovers much faster than 568-Ecad-H12, but it is important to note that this is still much slower for a lipid-conjugated dye in a normal fluid bilayer. The FRAPEvolve program calculates this sample's NBD-PC to have a diffusion coefficient of 0.04 $\mu m^2/s$. However, this calculation may not be accurate since the recovery at 2 minutes appears to show both a slow and fast moving lipid fraction. The 568-Ecad-H12 photobleaching shows fluidity at too slow of a timescale for the program to calculate; judging from the line profile, the diffusion coefficient may be one-tenth or smaller than that of the NBD-PC. This particular sample is relevant as it produced the cell results illustrated in figure 3.7 **C1**.

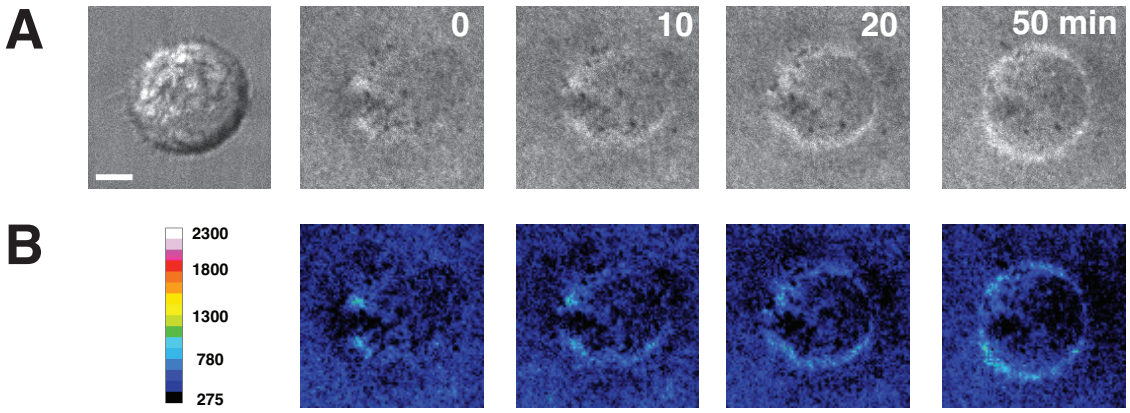

Figure 3.5 – MKN28 forming ring on low-fluidity 568-Ecad-H12. Time sequence of a cell remodeling 568-Ecad-H12 on a low-mobility DMPC surface. Time corresponds to start of movie, which begins 60 minutes after the addition of cells. Row **A** shows original images, and intensity is due to the fluorescence emitted from 568-Ecad-H12, except for the leftmost image, which is transmitted light. Row **B** shows the same fluorescence images after rescaling to correct for photobleaching and calibrating to TR bilayer standards. Values on the calibration bar denote molecules of 568-Ecad-H12 per μm^2. Scale bar, 5 μm.

With cell incubation and imaging being performed at 37 °C, the DPPC bilayers remained in a gel phase, showing no fluidity (no recovery of fluorescence after photobleaching). MKN28 cells adhered, but continued to show low rates of enriched adhesions, with only ~ 2% of the cells added forming such junctions. This number is from counting the cells in two separate experiments, and this low rate has been observed but not quantified in several other experiments.

One may think that the strong attachment of the cells to E-cadherin adsorbed glass would imply strong adhesion to the E-cad-DPPC surface and thus clustering or deformation of the protein distribution. However, the DPPC bilayer and E-cadherin adsorbed glass are different with respect to protein surface densities. The E-cadherin coated glass is likely saturated with protein, while the DPPC has a similar range of coverage as the DMPC and DOPC bilayers, given that the mole percentage of Ni-NTA-DOGS doped into the bilayers was kept at 4% across samples.

3.7 Differences in binding frequencies

As the results show, and also summarized in figure 3.6, the low mobility DMPC surface hosted the greatest number of 568-Ecad-H12 enriched cell adhesions (~54%), while cells formed such adhesions only 1 – 3% of the time on the other surfaces. These results suggest that a specific threshold of force is required for the enriched junctions, which presumably involve the formation of strand-swapped E-cadherin dimers. The high fluidity of the DOPC bilayer provides little resistance against a cell forming initial binding interactions with the surface 568-Ecad-

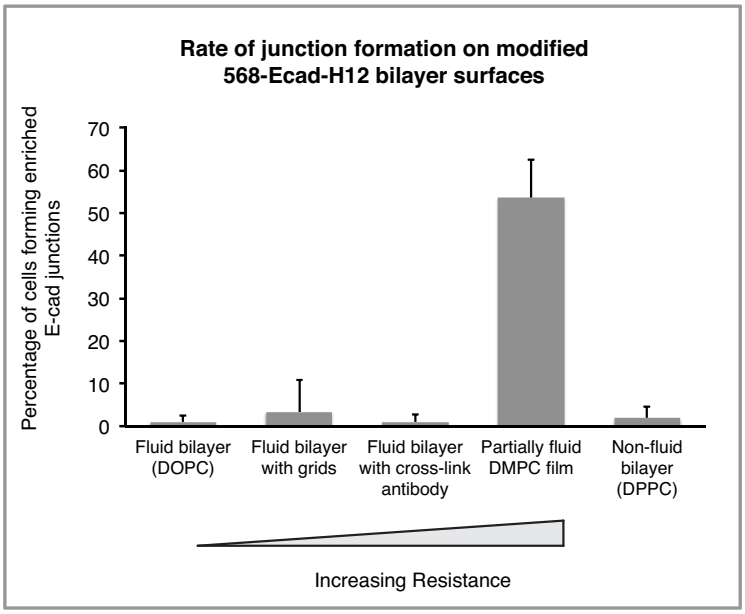

Figure 3.6 – Frequency of MKN28 adhesions on different 568-Ecad-H12 surfaces. Error bars show standard deviation of results. The surfaces were examined across 8, 5, 3, 4, and 2 separate experiments for DOPC, grids, cross-linking antibody, DMPC film, and DPPC, respectively. For each experiment, cells seeded in the sample were allowed to interact with the protein surface for 2 – 3 hours, and then were counted, or fixed and counted. In each experiment, 50 – 100 cells were examined. Cells showing an increased density of 568-Ecad-H12, as visible by epifluorescence within the contact region, were counted as having an enriched E-cadherin junction. In all samples, a large portion of cells adhered to the surface but did not show an increase in 568-Ecad-H12 surface density. This is likely a result of cell affinity to the protein-free Ni-NTA lipid head groups.

H12. The bilayer with grids provides resistance at micron-scale intervals, while allowing high fluidity elsewhere. Cross-linking with an antibody lowers the diffusion coefficient and thus increases the resistance across the surface, but not as much as the DMPC film, which appears to be within the range to trigger such E-cadherin junction assemblies. Cells adhere to the DPPC bilayer as would be expected from the protein adsorbed glass assay, but very few actively cluster the protein, suggesting that DPPC has a resistance too high to allow the same types of adhesions observed on DMPC.

The implications of force will be discussed after first addressing the physiological relevance of the E-cadherin adhesions observed.

3.8 Micro-architecture of the E-cadherin cell adhesions on DOPC and DMPC surfaces

To check the physiological relevance of the cell adhesions, cells showing enrichment of 568-Ecad-H12 on the DOPC or DMPC surfaces were fixed with paraformaldehyde and immunostained for certain binding partners of the adherens junction: F-actin, α-catenin, and intracellular E-cadherin. These were imaged with fluorescence microscopy, and the physical adhesion of the cell was imaged with reflection interference contrast.

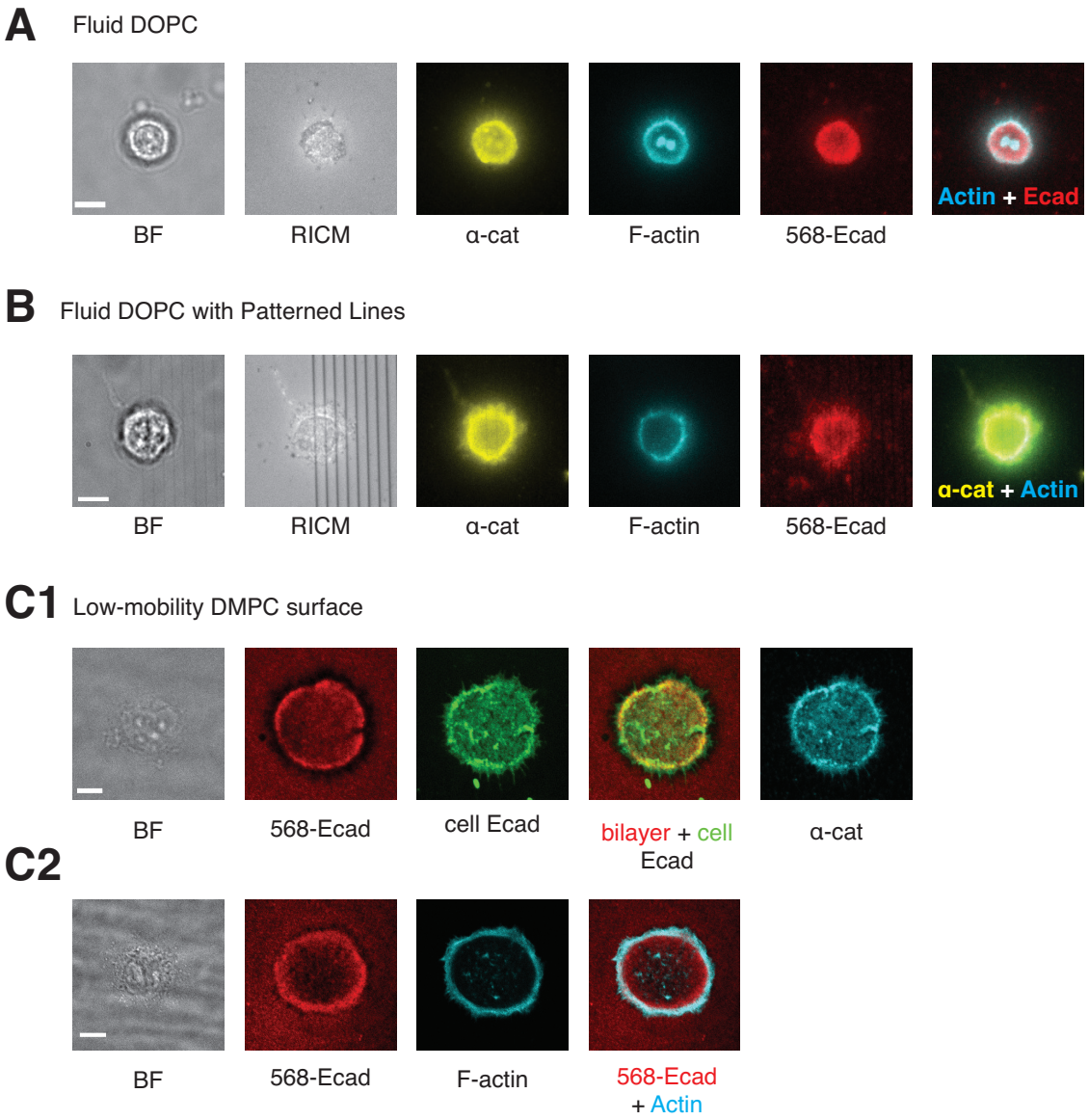

Figure 3.7 – MKN28 fluid and low-fluidity adhesion immunostaining. Scale bars, 5 μm.

However, RICM can only point out locations of adhesion. Immunostaining the E-cadherin binding partners highlights the reorganization of proteins within the cell that are known to strengthen and facilitate E-cadherin based cell-cell adhesion. The co-localization of enriched bilayer E-cadherin with cellular E-cadherin, seen in figure 3.7 C1, is a signature of trans-dimer formation. F-actin staining of the junctions formed from both fluid DOPC and the low-mobility DMPC (figure 3.7 A, B, C2) shows an annulus on the periphery of the enriched E-cadherin zone, and occasionally co-localization within (such as figure 3.7 A). The reorganization of the actin cytoskeleton is characteristic of intercellular adhesions [67]. More specifically, this type of peripheral actin ring has been observed previously with a cell's EphA2 receptor on a fluid bilayer of its EphrinA1 ligand [33, 68]. EphA2 dynamically associates with the F-actin cytoskeleton during enrichment of the bilayer EphrinA1, and dissociates upon reaching a few microns within the cell adhesion site. Though the behavior of actin dynamics in E-cadherin junction formation is out of the scope of this study, the immediate similarities with the EphrinA1-EphA2 bilayer system suggests that the same interaction is at work: bilayer E-cadherin is bound to cellular E-cadherin through filopodia retraction, and is pulled to the periphery of the cell by the indirect connection with F-actin. Once there, the connection with F-actin is broken, but the trans-dimerization remains. In the case of low mobility DMPC, this process results in E-cadherin enrichment at the cell periphery, as it does not diffuse towards the center of the cell adhesion at the timescale investigated. In the rare adhesion events on DOPC, the E-cadherin is likely clustered from the periphery as well, and the difference in phenotype is due to the cell contracting on a fluid surface (as mentioned previously), and the ability of the E-cadherin trans-dimers to diffuse towards the center of the adhesion.

The staining with α-catenin shows more about the link between actin and the cell's E-cadherin. Co-localization of α-catenin with E-cadherin and F-actin is observed at cell-cell contacts. Furthermore, this co-localization shows that the formation of the E-cadherin adhesion has triggered biochemical changes within the cell for the recruitment of binding partners. In the immunostaining images shown in figure 3.7 A, B, C1; α-catenin generally co-localizes with the actin annulus and peripheral E-cadherin. This supports the hypothesis that E-cadherin trans-dimers are formed at the periphery of the cell by actin association and then dissociate from actin within the adhesion. Since α-catenin is involved in the linkage of E-cadherin with actin (discussed in section 1.2.2 on page 4), the severed connection allows α-catenin to diffuse within the cytoplasm, away from the site of adhesion.

Overall, these cell staining results confirm that the synthetic E-cadherin membrane display can mimic the E-cadherin junction formed between two cells, using both fluid and low-mobility surfaces. However, the question of adhesion rates remains, and this can be answered by looking closely at the mechanisms involved in the development of enriched E-cadherin junctions.

3.9 Mechanisms of selective E-cadherin adhesion formation

3.9.1 Filopodia retraction reveals force dependence of E-cadherin adhesion

Live cell imaging of E-cadherin enrichment on low-mobility DMPC surfaces showed active filopodia extension and retraction events. Such active cytoskeleton remodeling, in the form of filopodia or lamellipodia, has been observed in the development of cadherin-based cell contacts [25, 27]. Following the retraction events by RICM confirmed their role in the active transport and enrichment of bilayer E-cadherin (figure 3.8). On the low-mobility DMPC with E-cadherin, the filopodia retracted with an average velocity of 12 ± 3 nm/s. The DOPC protein bilayer showed much faster filopodia retraction velocities of 180 ± 120 nm/s, which did not correspond to any change in 568-Ecad-H12 distribution.

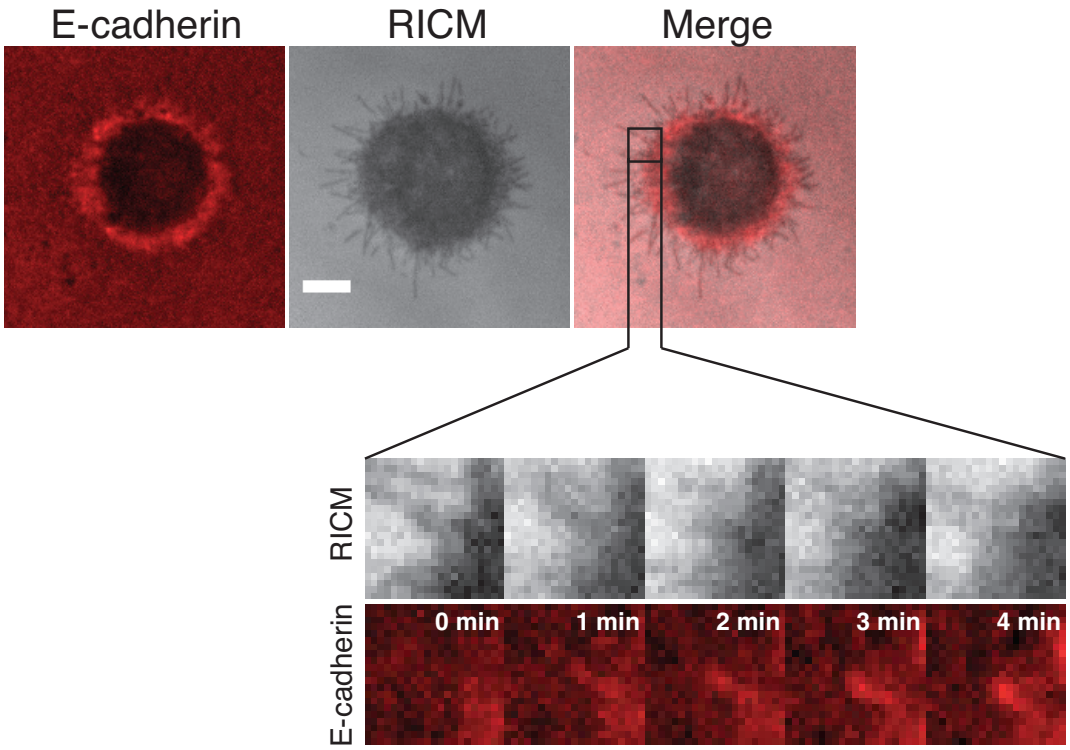

Figure 3.8 – Filopodia retraction and protein enrichment on low-mobility E-cadherin surface. The cutout shows filopodia retraction, observed in RICM, corresponding with the increased surface density of 568-Ecad-H12. The average retraction velocity on the low-mobility DMPC was observed to be 12 ± 3 nm/s. Scale bar, 5 μm.

The filopodia-driven enrichment of figure 3.8 seems to point to force (from the drag of the viscous DMPC surface) or increased surface density as the physical trigger of E-cadherin adhesion formation. Force can be better addressed by considering the filopodia retraction speeds and diffusion coefficients. Since the 568-Ecad-H12 diffuses as a single species on the DOPC

bilayer, an upper limit of the possible drag forces on retracting filopodia can be calculated by applying the Einstein-Smoluchowski (E-S) form of the fluctuation-dissipation theorem:

$$D = \mu k_B T. \tag{3.1}$$

For a given diffusion coefficient and temperature of a fluid, this equation gives the mobility μ. This is the relative velocity of a sphere in a surrounding fluid divided by the force required to keep it at that velocity (ie. drag). Substituting this relation, $\mu = \frac{V}{F}$, into equation 3.1 produces

$$F = \frac{V k_B T}{D}. \tag{3.2}$$

The values V = 180 nm/s, $k_B T$ = 4.28 pN$\cdot$nm (at 37°C), and D = 1.5 μm^2/s are plugged into equation 3.2, producing F = 0.5 fN. This represents a small drag force created by the interaction of the filopodia's E-cadherin with the 568-Ecad-H12 in the DOPC bilayer, and would be the upper limit of force on trans-dimers, if the drag force was caused solely by the trans-interactions between E-cadherin on the filopodia with 568-Ecad-H12 on the bilayer.

There is a temptation to apply a similar analysis to the results of the DMPC surface. Estimating the diffusion coefficient from the DMPC FRAP image (figure 3.4 on page 41), using the Soumpasis approximation (equation 2.1) gives D = 0.005 μm^2/s. Combining with equation 3.2 gives a force of 0.01 pN, which is much lower than the expected 30 pN catch bond force. However, substituting $\mu = \frac{V}{F}$ into equation 3.1 requires that all of the 568-Ecad-H12 molecules diffuse at D for the duration of the experiment. For DOPC, which was shown earlier to have a single oligomeric species diffusion of 568-Ecad-H12, this requirement is met. But for DMPC, the significant enrichment of protein underneath the filopodia would cause a drastic decrease in the already low 568-Ecad-H12 mobility, which would invalidate the linear relation between μ and D and make the E-S relation inapplicable. Furthermore, the low mobility DMPC surface was never shown to exhibit single species diffusion, as its diffusion was so slow as to make a rigorous FCS measurement impossible. Thus, even though the 568-Ecad-H12 on DMPC showed slow recovery after photobleaching, assigning a value of D may be too inaccurate. In any case, it is likely that the low mobility DMPC supplies enough drag for the retracting filopodia to nucleate strand-swapped dimers with the presented 568-Ecad-H12.

At the other extreme, DPPC does not show a significant 568-Ecad-H12 surface density increase by the cell, likely due to the weakness of the bond in the strand-swapped trans-dimer. The formation of protein enrichment relies on the lateral translocation of trans-dimers, and the gel-phase DPPC bilayer is probably too resistive to allow the cell to cluster the trans-dimers without their dissociation. It would seem reasonable, then, to mix lipids of high and low fluidity to achieve surfaces with fluidities around that of the DMPC film, in order to determine a specific range that activates E-cadherin adhesion. Unfortunately, the mobilities of lipid mixtures cannot be extrapolated that way, as such a mixture may result in a bilayer with separate lipid domains. This result would be non-ideal for observing cell behavior as the location and size of

the lipid domains could not be controlled easily. Physical characterization of the bilayer would be difficult for the same reason of heterogeneity.

3.9.2 Passive adhesion does not form enriched junctions when starting with low or moderate surface density

Despite the presumed roles of E-cadherin force dependence and fluidity in adhesion formation, there are other characteristics of the protein to take into account. To be more complete, an explanation of the filopodia-driven enrichment must consider that E-cadherin adhesion can occur among passive surfaces, as described by the diffusion trap model. The contribution of passive E-cadherin binding in the case of the cell observations can be determined by looking at the purely passive adhesion that occurs between E-cadherin decorated GUV and supported lipid bilayers.

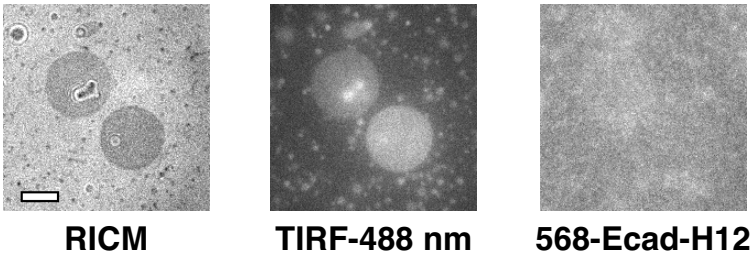

Figure 3.9 – Binding between GUV and SLB, both of 568-Ecad-H12 on DOPC. GUV lipids consist of 2% Ni-NTA-DOGS, 1% NBD-PC, and 97% DOPC. The lipid bilayer is 2% Ni-NTA-DOGS, 1% Marina Blue-DHPE, and 97% DOPC. GUV were formed in 100 mM sucrose, and added to a bilayer with a $\sim$ 276 Ecad/μm^2 surface density and with 568-Ecad-H12 in a saline-free tris buffer with 1 mM $CaCl_2$. GUV were incubated at RT for 38 minutes, and show adhesion via RICM, but do not show an enriched contact of 568-Ecad-H12. The 488-TIRF image shows the part of the vesicle within 100 nm of the bilayer. The small spots in the RICM and 488-TIRF images are not bilayer aggregates but small vesicles. The fluidity of the bilayer had been confirmed with FRAP. Scale bar, 5 μm.

As mentioned earlier in section 1.3.2, E-cadherin binding among GUV and with lipid bilayers have been examined in previous experiments but did not look at changes in surface density at contact regions. In this current study, GUV and lipid bilayers, both with 568-Ecad-H12, 2% Ni-NTA-DOGS, and fluid DOPC, frequently exhibited adhesion at moderate surface densities (figure 3.9). This adhesion was visible from RICM, but did *not* include enrichment of 568-Ecad-H12 surface density at the contact region. However, data from Professor Michael Dustin's lab with the same 568-Ecad-H12 on both fluid vesicles and fluid lipid bilayers at higher surface densities (500 – 5,000 Ecad/μm^2) did show an enrichment of E-cadherin at the sites of adhesion [69].

These observations of passive adhesions appear to disagree with the cell observations discussed earlier and illustrated in figure 3.10: cells rarely assemble enriched E-cadherin junctions

with fluid DOPC, but vesicles with E-cadherin at a sufficiently high surface density can reliably form such junctions by passive binding. However, these results are not necessarily exclusive of each other; the apparent difference can be rectified by considering the initial conditions required for the diffusion trap mechanism and the time needed for stable E-cadherin binding.

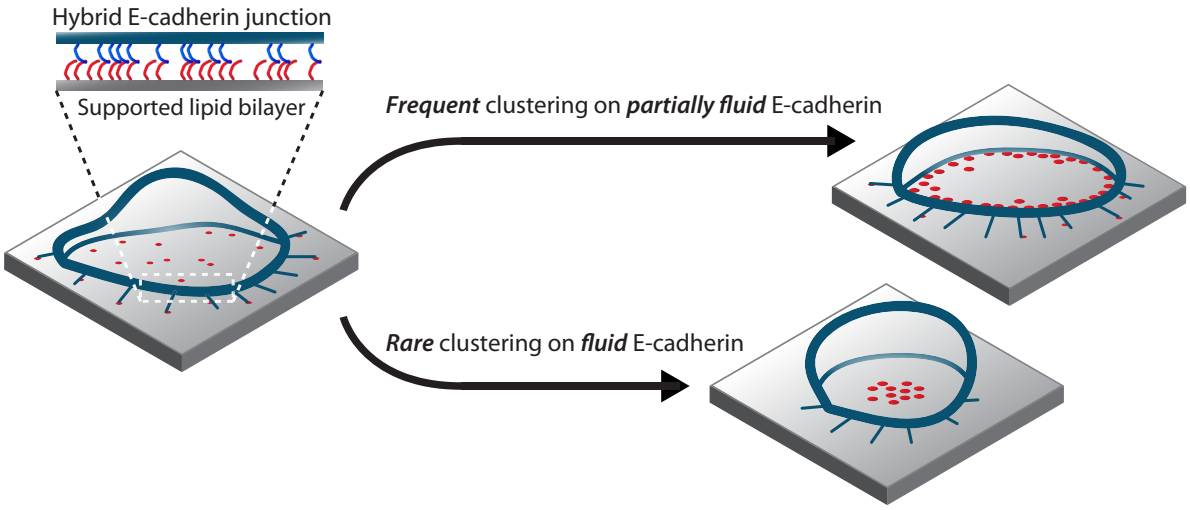

Figure 3.10 – Illustration of cell behavior observed between DOPC and DMPC.

For the diffusion trap to work, it requires a high initial surface density and a contact between two surfaces that is free from shear or other large movements. GUV added to a lipid bilayer can provide this type of stable contact, as they can sink to the bottom of the solution and stay put as long as the sample is kept still. To date, however, E-cadherin adhesions between GUV and a bilayer versus cells and a bilayer have not been directly compared with respect to density enrichment. Passive E-cadherin adhesions are probably less dense than active cell-driven adhesions, given that the surface density can be increased several-fold by retracting filopodia.

3.9.3 Time dependence

Not only does the development of passive E-cadherin adhesion depend on a degree of stability for the diffusion trap to stabilize diffusing trans-dimers, it also depends on stability for those initially contacting dimers to evolve into a strand-swapped dimer configuration. This time dependence was observed through the single E-cadherin bond force measurements of Rakshit et al. as described earlier in section 1.3.3.

Again, GUVs and lipid bilayers displaying freely diffusing E-cadherin illustrate the role of time dependence. Just as in the case of the diffusion trap, GUV can sink and rest on the surface of an E-cadherin bilayer, allowing time for E-cadherin trans-dimers to develop into strand-swapped dimers. The enrichment of E-cadherin at the contact is able to develop passively, without force or cell activity such as filopodia retraction, provided that the starting density is sufficiently high.

In the case of cells adhering to low mobility DMPC, the time dependence comes into play with both the initially low diffusion rate of the surface, and the further decreased diffusion rate of the protein within enriched clusters. The slow translation gives time for the cell's E-cadherin binding with 568-Ecad-H12 to develop into strand-swapped dimers, and simultaneously allows newer binding to occur through the force dependent catch bond.

3.9.4 Current model: density and force allow active cell processes to nucleate adhesion

MKN28 cells show a low rate of binding on DOPC surfaces because the cell interaction is anything but passive. Small contacts of E-cadherin trans-dimers may form, but the ongoing contractions and filopodia activity of the cell likely do not allow a long enough time for other weakly bound trans-dimers to diffuse into the stabilizing contact region. The data show that even restricting the translation of the protein by nano-patterned gridlines or a clustering antibody is not sufficient to overcome the destabilizing conditions of both high bilayer diffusion rate and cell movement.

Obviously, the low-mobility DMPC surface provides the conditions that assist E-cadherin adhesion. The slow fluidity of the bilayer-bound 568-Ecad-H12 gives more time for the cell's E-cadherin to interact. The enrichment created by the retracting filopodia probably decreases the protein's fluidity even more—the 568-Ecad-H12 molecules are likely jammed together into a thick plaque. This mass of protein would be able to provide both the resistance for catch bond development as well as the necessary contact time for strand-swapped dimers to form. Thus, the rate of enriched adhesion formation is much greater on the low mobility DMPC surface, due to the force and density it supplies to retracting cell filopodia. The experiments of this study cannot distinguish if the effect is exclusively a result of the E-cadherin force dependence or the protein's surface density. It may be that both are required given that the two properties are simultaneously active during filopodia-driven E-cadherin enrichment.

The requirements for E-cadherin cell adhesion described here, low fluidity and active filopodia retraction, is contradictory with respect to the binding of a model cell surface protein. With a stereotypical protein surface receptor, high fluidity increases the number of receptor-ligand interactions that lead to binding, without the cell having to act in a certain way. The peculiar requirements of E-cadherin adhesion likely arise from the relative weakness of the E-cadherin trans-dimer and its force-dependent binding modes.

3.10 Summary of cell response

MKN28 cells were observed to form adhesions of enriched 568-Ecad-H12 on both fluid DOPC and a low-mobility DMPC surface. Staining the cells of both surfaces revealed co-localization of α-catenin and intercellular E-cadherin. Furthermore, F-actin was reorganized into a cortical ring. All of these characteristics are indicative of an E-cadherin mediated adhesion *in vivo*,

and thus, the supported lipid bilayer is a successful application to simulate and fully image E-cadherin junction formation and dynamics.

Beyond that, the use of different lipids revealed that the rate of E-cadherin junction formation on a low-mobility DMPC lipid surface was far higher than with the surfaces of fluid DOPC, DOPC with diffusion barriers, or DOPC with the application of a protein-clustering antibody. This is unexpected as a fluid surface would have a higher rate of protein-protein collisions, which should lead to a higher rate of binding. Additionally, cell membranes themselves are inherently fluid. Live cell imaging of E-cadherin junction formation showed that the tips of retracting filopodia correspond to points of enriched 568-Ecad-H12 density. This is likely due to a force activation of trans-binding created by the increase in protein density by weaker interactions, combined with the low mobility of the DMPC surface. These two factors afford the surface-bound E-cadherin enough time to form stable trans and cis-interactions. With fluid DOPC, the rate of diffusion is much faster, and the cell's filopodia activity likely perturbs the binding that would otherwise occur. Diffusion barriers and dimerizing antibodies do not overcome the influence of fast diffusion, and the DPPC bilayer provides too much resistance against the force dependent binding and translocation of E-cadherin clusters.

Chapter 4

Future directions

4.1 SNAP-tag DNA attachment scheme as an alternative to His-tag Ni-NTA

Earlier sections have discussed three techniques that have been used to attach E-cadherin to the lipid bilayer surface: GPI anchoring, biotin-streptavidin, and polyhistidine tag. The polyhistidine tag was used with the extracellular domain of E-cadherin for physical characterization of the protein's density and fluidity, and then its response to cell binding. Though this attachment has been fruitful for this study, it presents a few drawbacks that can be addressed by using SNAP-tag DNA as an alternative.

Firstly, the MKN28 cells used in this study occasionally showed an affinity to the Ni-NTA-DOGS lipid surface, and these adhesions would occur to the exclusion of 568-Ecad-H12 protein (see figure 4.1). Such exclusion spots could be moved around by the cell, and the presence of fluorescent lipid dye underneath (NBD-PC or Marina Blue-DHPE, for example), indicated that the cells were adhering to the lipids without rupturing the bilayer surface or coming into contact with the glass coverslip. When no protein was added, cells would still adhere to the 4% Ni-NTA-DOGS lipid surface, but not to a bilayer of 100% DOPC, indicating that the Ni-NTA-DOGS lipid molecules were responsible.

The second downside with the polyhistidine Ni-NTA attachment scheme is the lack of protein stability in cell medium. Nye et al. have shown that GFP-H10 on a 2% Ni-NTA-DOGS bilayer can persist on the surface for up to 23 hours with only slow desorption, in normal saline buffer. However, experiments with EphrinA1-eYFP-H10 or E-cadherin variants with polyhistidine termini have shown fast desorption in cell experiments that use mammalian cell media, such as RPMI or DMEM. Often, the majority of the protein is desorbed 45 – 60 minutes after adding the cell media to the protein bilayer. This causes fluorescence intensity loss of free protein on the bilayer, but not always to the protein that the cells adhere. Due to this protein loss, cells can appear to enrich protein at a greater density, especially if this density is calibrated against the free protein surface with the idea of accommodating photo-bleaching.

The exact cause of the protein desorption is not understood. The obvious theory would be

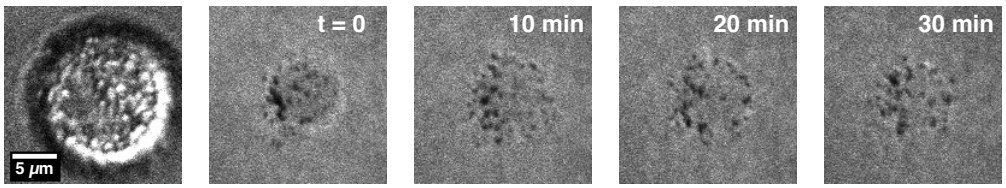

Figure 4.1 – Non-specific binding between MKN28 and Ni-NTA-DOGS. 568-Ecad-H12 bilayer samples were prepared with 4% Ni-NTA-DOGS and 96% DOPC, according to previously described procedures. MKN28 cells were incubated for 50 minutes before starting time-lapse imaging; time denotes start of imaging and the bright field image shown is at t = 0 min. The dark spots in the 568-Ecad-H12 images are areas of excluded protein. These are created by the cell and appear to move over the course of the time-lapse, giving evidence that the 568-Ecad-H12 is able to diffuse into previous locations of the spots, and showing that the spots contain an unruptured bilayer surface. Aggregated protein or a hole in the lipid bilayer would not move. These depleted areas are likely caused by the cell interacting with the Ni-NTA lipid head-groups that are not chelated to protein.

that the L-histidine supplemented in the media competes with the polyhistidine tail of the protein of interest, though other components of the media could potentially interfere. Histidine-free media can be acquired, but given the other disadvantages of the his-tag Ni-NTA system, it has not been worth pursuing at this point. In the cell experiments of Chapter 3, a HEPES buffer supplemented with salts and glucose at concentrations similar to RPMI was used in place of cell media, for the purpose of protein attachment stability. If the cells respond differently in fully-supplemented RPMI media compared to the imaging buffer is unknown. However, cell incubation times are probably short enough with this study to create only negligible differences.

The third downside of the polyhistidine attachment to Ni-NTA-DOGS is its incompatibility with metal chelators (such as EDTA or EGTA), due to the dependence on Ni^{2+}. This prevents "calcium-switch" experiments to be performed with cells adhering to cadherin proteins attached through the Ni-NTA. This type of experiment involves incubation with a metal chelator to remove Ca^{2+} from solution, which disables the calcium-dependent adhesion from cadherins. Then, incubation with an excess of Ca^{2+} restores the adhesion. The "calcium-switch" experiment is used with cadherin-expressing cells or cadherin-coated beads to test both the activity and specificity of cadherin binding. This would be a useful control for a cadherin bilayer system with an attachment scheme immune to added metal chelators.

The SNAP-tag DNA attachment to the bilayer surface requires a few more steps compared to the his-tag Ni-NTA method, but overcomes the three disadvantages listed above, as well as those of the other bilayer attachment schemes. Using the SNAP-tag requires incorporating the SNAP-tag domain into the sequence of the protein of interest. This domain is a mutated form of human O^6-alkylguanine-DNA alkyltransferase, with a size of 20 kDa, and its interior thiol group forms a covalent bond with a benzylguanine group [70]. For the bilayer attachment, outlined in figure 4.2, the protein of interest is expressed as a genetic fusion of the SNAP domain and a polyhistidine tag. The polyhistidine tag, in this case, is used only for the protein purifi-

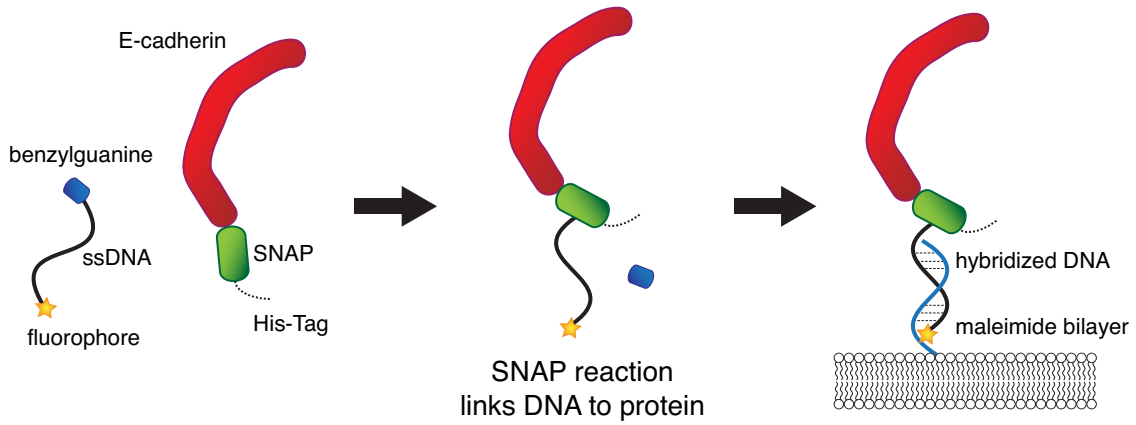

Figure 4.2 – Attaching E-cadherin to the bilayer with SNAP-tag DNA. A fusion protein of the E-cadherin extra-cellular domain and SNAP-tag is expressed and purified by Ni-NTA affinity chromatography. Single-strand DNA functionalized with benzylguanine at the 5' end, and with a fluorophore at the 3' end, reacts with the SNAP-tag domain of the E-cadherin protein construct. The ssDNA hybridizes with a fluid DNA bilayer that was created by reacting maleimide lipid head-groups with thiol-functionalized ssDNA.

cation. Single-stranded DNA functionalized with a benzylguanine group at the 5' end, and a fluorophore at the 3' end, reacts and attaches to the SNAP domain, leaving the fluorophore intact. A bilayer is prepared with a certain percentage of maleimide lipids, and reacted with thiol-functionalized ssDNA, which attaches the ssDNA to the lipid surface while maintaining a high degree of fluidity [71]. As the two ssDNA are complementary sequences, they hybridize when the protein-SNAP-tag-DNA is added to the bilayer, creating a stable linkage.

The SNAP-tag DNA attachment has extra specificity due to the reliance on hybridizing DNA sequences, which is advantageous for attaching two or more different proteins on the bilayer at equivalent surface densities. With other attachment schemes, differences in protein size may lead to smaller proteins diffusing to the bilayer surface and attaching faster than larger proteins.

4.2 Cross-talk between EphA2 and E-cadherin

EphA2 is a receptor tyrosine kinase over-expressed in 40% of human breast cancers [72], and mammary epithelia cells, when transfected to over-express EphA2, become metastatic [73]. The primary ligand of EphA2, named EphrinA1, has been tethered to a lipid bilayer. When human breast cancer cells were cultured on the surface, micron-sized areas of EphrinA1 enrichment were formed. These EphrinA1-EphA2 signaling complexes were transported to the center of the cell adhesion to an extent proportional to the cell's invasive character, highlighting a characteristic of its cell-driven spatial organization [33].

E-cadherin and EphA2 have complementary roles in conferring or limiting the invasive characteristics of cancer cells, and have furthermore been found to interact in multiple ways.

Zantek et al. found that EphA2 requires E-cadherin adhesion at cell-cell contacts for proper EphA2-EphrinA1 functioning [5]. Similarly, Orsulic and Kemler observed changes in EphA2 distribution on the cell surface when E-cadherin expression was knocked down [74]. Looking instead at EphA2 expression levels, Fang et al. found that EphA2 over-expression weakened E-cadherin adhesions without decreasing the overall expression levels of E-cadherin and its binding partners. Thus, the authors postulated that the destabilization occurred from the redistribution of E-caderhin on the cell surface [75].

These conclusions are not entirely incompatible with each other, and suggest that cell junction stability comes from a balance between EphA2 and E-cadherin activity. However, all three studies came before the discovery of EphA2-EphrinA1 spatial regulation, and fail to consider synthetic membranes as a technique of studying epithelial cell contacts. The conclusions regarding EphA2 and E-cadherin interactions describe phenomena of junction assembly and disassembly that could be observed directly with bilayers displaying both E-cadherin and EphrinA1. Potential experiments should look at the differences in the spatial distributions of the two proteins across cancer cell lines of different invasion potential, as well as across a particular cell line with modified expression levels of E-cadherin and EphA2.

Bibliography

1. Wendt, M. K., Taylor, M. A., Schiemann, B. J. & Schiemann, W. P. Down-regulation of epithelial cadherin is required to initiate metastatic outgrowth of breast cancer. *Molecular Biology of the Cell* **22,** 2423–2435 (July 2011).
2. Frixen, U. *et al.* E-cadherin-mediated cell-cell adhesion prevents invasiveness of human carcinoma cells. *The Journal of Cell Biology* **113,** 173–185 (Apr. 1991).
3. Takeichi, M. Functional correlation between cell adhesive properties and some cell surface proteins. *The Journal of Cell Biology* **75,** 464–474 (Nov. 1977).
4. Powell, K. The sticky business of discovering cadherins. *The Journal of Cell Biology* **170,** 514–514 (Aug. 2005).
5. Zantek, N. D. *et al.* E-Cadherin Regulates the Function of the EphA2 Receptor Tyrosine Kinase. *Cell Growth Differentiation* **10,** 629–638 (Sept. 1999).
6. Hong, S., Troyanovsky, R. B. & Troyanovsky, S. M. Binding to F-actin guides cadherin cluster assembly, stability, and movement. *The Journal of Cell Biology* **201,** 131–143 (Apr. 2013).
7. Sivasankar, S., Zhang, Y., Nelson, W. J. & Chu, S. Characterizing the initial encounter complex in cadherin adhesion. *Structure* **17,** 1075–1081 (Aug. 2009).
8. Brasch, J., Harrison, O. J., Honig, B. & Shapiro, L. Thinking outside the cell: how cadherins drive adhesion. *Trends in Cell Biology* **22,** 299–310 (June 2012).
9. Vendome, J. *et al.* Molecular design principles underlying β-strand swapping in the adhesive dimerization of cadherins. *Nature Structural & Molecular Biology* **18,** 693–700 (June 2011).
10. Shi, Q., Chien, Y.-H. & Leckband, D. Biophysical Properties of Cadherin Bonds Do Not Predict Cell Sorting. *The Journal of Biological Chemistry* **283,** 28454–28463 (Oct. 2008).
11. Katsamba, P. *et al.* Linking molecular affinity and cellular specificity in cadherin-mediated adhesion. *Proceedings of the National Academy of Sciences* **106,** 11594–11599 (July 2009).
12. Pabbisetty, K. B. *et al.* Kinetic analysis of the binding of monomeric and dimeric ephrins to Eph receptors: Correlation to function in a growth cone collapse assay. *Protein Science* **16,** 355–361 (2007).

13. Urbinati, C. *et al.* $\alpha_v\beta_3$-integrin-dependent activation of focal adhesion kinase mediates NF-κB activation and motogenic activity by HIV-1 Tat in endothelial cells. *Journal of Cell Science* **118,** 3949–3958 (Sept. 2005).

14. Harrison, O. J. *et al.* The extracellular architecture of adherens junctions revealed by crystal structures of type I cadherins. *Structure* **19,** 244–256 (Feb. 2011).

15. Harrison, O. J. *et al.* Two-step adhesive binding by classical cadherins. *Nature Structural & Molecular Biology* **17,** 348–357 (Mar. 2010).

16. Wu, Y. *et al.* Cooperativity between trans and cis interactions in cadherin-mediated junction formation. *Proceedings of the National Academy of Sciences* **107,** 17592 –17597 (Oct. 2010).

17. Wu, Y., Vendome, J., Shapiro, L., Ben-Shaul, A. & Honig, B. Transforming binding affinities from three dimensions to two with application to cadherin clustering. *Nature* **475,** 510–513 (July 2011).

18. Weis, W. I. & Nelson, W. J. Re-solving the cadherin-catenin-actin conundrum. *The Journal of Biological Chemistry* **281,** 35593–35597 (Nov. 2006).

19. Nelson, W. J. Regulation of cell-cell adhesion by the cadherin-catenin complex. *Biochemical Society Transactions* **36,** 149–155 (Apr. 2008).

20. Kametani, Y. & Takeichi, M. Basal-to-apical cadherin flow at cell junctions. *Nature Cell Biology* **9,** 92–98 (Jan. 2007).

21. Heuberger, J. & Birchmeier, W. Interplay of Cadherin-Mediated Cell Adhesion and Canonical Wnt Signaling. *Cold Spring Harbor Perspectives in Biology* **2,** a002915 (2010).

22. Wheelock, M. J. & Johnson, K. R. Cadherin-mediated cellular signaling. *Current Opinion in Cell Biology* **15,** 509–514 (Oct. 2003).

23. Zaidel-Bar, R. Cadherin adhesome at a glance. *Journal of Cell Science* **126,** 373–378 (Jan. 2013).

24. Hong, S., Troyanovsky, R. B. & Troyanovsky, S. M. Spontaneous assembly and active disassembly balance adherens junction homeostasis. *Proceedings of the National Academy of Sciences* **107,** 3528 –3533 (Feb. 2010).

25. Vasioukhin, V., Bauer, C., Yin, M. & Fuchs, E. Directed Actin Polymerization Is the Driving Force for Epithelial Cell–Cell Adhesion. *Cell* **100,** 209–219 (Jan. 2000).

26. Perez-Moreno, M., Jamora, C. & Fuchs, E. Sticky Business: Orchestrating Cellular Signals at Adherens Junctions. *Cell* **112,** 535–548 (Feb. 2003).

27. Gavard, J. *et al.* Lamellipodium extension and cadherin adhesion: two cell responses to cadherin activation relying on distinct signalling pathways. *Journal of Cell Science* **117,** 257–270 (Jan. 2004).

28. Perez, T. D., Tamada, M., Sheetz, M. P. & Nelson, W. J. Immediate-Early Signaling Induced by E-cadherin Engagement and Adhesion. *J. Biol. Chem.* **283,** 5014–5022 (Feb. 2008).

29. Puech, P.-H., Feracci, H. & Brochard-Wyart, F. Adhesion between Giant Vesicles and Supported Bilayers Decorated with Chelated E-Cadherin Fragments. *Langmuir* **20,** 9763–9768 (Oct. 2004).

30. Fenz, S. F., Merkel, R. & Sengupta, K. Diffusion and intermembrane distance: case study of avidin and E-cadherin mediated adhesion. *Langmuir* **25,** 1074–1085 (Jan. 2009).

31. Rakshit, S., Zhang, Y., Manibog, K., Shafraz, O. & Sivasankar, S. Ideal, catch, and slip bonds in cadherin adhesion. *Proceedings of the National Academy of Sciences* **109,** 18815–18820 (Nov. 2012).

32. Borghi, N., Lowndes, M., Maruthamuthu, V., Gardel, M. L. & Nelson, W. J. Regulation of cell motile behavior by crosstalk between cadherin- and integrin-mediated adhesions. *Proceedings of the National Academy of Sciences* **107,** 13324–13329 (June 2010).

33. Salaita, K. *et al.* Restriction of Receptor Movement Alters Cellular Response: Physical Force Sensing by EphA2. *Science* **327,** 1380–1385 (Mar. 2010).

34. Sivasankar, S, Brieher, W, Lavrik, N, Gumbiner, B & Leckband, D. Direct molecular force measurements of multiple adhesive interactions between cadherin ectodomains. *Proceedings of the National Academy of Sciences* **96,** 11820–11824 (Oct. 1999).

35. Hartman, N. C., Nye, J. A. & Groves, J. T. Cluster size regulates protein sorting in the immunological synapse. *Proceedings of the National Academy of Sciences* **106,** 12729 –12734 (2009).

36. Xu, Q., Lin, W.-C., Petit, R. S. & Groves, J. T. EphA2 Receptor Activation by Monomeric Ephrin-A1 on Supported Membranes. *Biophysical Journal* **101,** 2731–2739 (Dec. 2011).

37. Andreasson-Ochsner, M. *et al.* Single cell 3-D platform to study ligand mobility in cell-cell contact. *Lab on a Chip* **11,** 2876–2883 (Sept. 2011).

38. Charnley, M., Kroschewski, R. & Textor, M. The study of polarisation in single cells using model cell membranes. *Integrative Biology: Quantitative Biosciences from Nano to Macro* **4,** 1059–1071 (Sept. 2012).

39. Lin, W.-C., Yu, C.-H., Triffo, S. & Groves, J. T. Supported Membrane Formation, Characterization, Functionalization, and Patterning for Application in Biological Science and Technology. *Current Protocols in Chemical Biology* **2,** 235–269 (2010).

40. Perez, T. D., Nelson, W. J., Boxer, S. G. & Kam, L. E-Cadherin Tethered to Micropatterned Supported Lipid Bilayers as a Model for Cell Adhesion. *Langmuir* **21,** 11963–11968 (Dec. 2005).

41. Laitinen, O. H., Hytönen, V. P., Nordlund, H. R. & Kulomaa, M. S. Genetically engineered avidins and streptavidins. *Cellular and Molecular Life Sciences: CMLS* **63,** 2992–3017 (Dec. 2006).

42. Yu, C.-H., Law, J. B. K., Suryana, M., Low, H. Y. & Sheetz, M. P. Early integrin binding to Arg-Gly-Asp peptide activates actin polymerization and contractile movement that stimulates outward translocation. *Proceedings of the National Academy of Sciences* **108,** 20585–20590 (Dec. 2011).

43. Nye, J. A. & Groves, J. T. Kinetic Control of Histidine-Tagged Protein Surface Density on Supported Lipid Bilayers. *Langmuir* **24,** 4145–4149 (Apr. 2008).

44. Tenchov, B. G., Yanev, T. K., Tihova, M. G. & Koynova, R. D. A probability concept about size distributions of sonicated lipid vesicles. *Biochimica et Biophysica Acta* **816,** 122–130 (June 1985).

45. Pietsch, G. J., Kohler, U. & Henzler, M. Chemistry of silicon surfaces after wet chemical preparation: A thermodesorption spectroscopy study. *Journal of Vacuum Science & Technology B: Microelectronics and Nanometer Structures* **12,** 78–87 (1994).

46. Parisini, E., Higgins, J. M. G., Liu, J.-H., Brenner, M. B. & Wang, J.-H. The crystal structure of human E-cadherin domains 1 and 2, and comparison with other cadherins in the context of adhesion mechanism. *Journal of Molecular Biology* **373,** 401–411 (Oct. 2007).

47. Saffman, P. G. & Delbrück, M. Brownian motion in biological membranes. *Proceedings of the National Academy of Sciences* **72,** 3111 –3113 (1975).

48. Soumpasis, D. M. Theoretical analysis of fluorescence photobleaching recovery experiments. *Biophysical Journal* **41,** 95–97 (Jan. 1983).

49. Phillips, R. & Theriot, J. *Physical biology of the cell* (Garland Science, New York, 2008).

50. Jacobs, D. CMSC 828. Advanced Topics in Information Processing: Image Segmentation. Diffusion Processes. *University of Maryland* 2012. <`http://www.cs.umd.edu/~djacobs/CMSC828seg/Diffusion.pdf`>.

51. Enderlein, J., Gregor, I., Patra, D., Dertinger, T. & Kaupp, U. B. Performance of fluorescence correlation spectroscopy for measuring diffusion and concentration. *ChemPhysChem* **6,** 2324–2336 (Nov. 2005).

52. Chiantia, S., Ries, J. & Schwille, P. Fluorescence correlation spectroscopy in membrane structure elucidation. *Biochimica et Biophysica Acta* **1788,** 225–233 (Jan. 2009).

53. Benda, A. *et al.* How To Determine Diffusion Coefficients in Planar Phospholipid Systems by Confocal Fluorescence Correlation Spectroscopy. *Langmuir* **19,** 4120–4126 (May 2003).

54. Sezgin, E. & Schwille, P. Fluorescence Techniques to Study Lipid Dynamics. *Cold Spring Harbor Perspectives in Biology* **3,** a009803 (Nov. 2011).

55. Humpolí˘cková, J. *et al.* Probing Diffusion Laws within Cellular Membranes by Z-Scan Fluorescence Correlation Spectroscopy. *Biophysical Journal* **91,** L23–L25 (Aug. 2006).

56. Manz, B. N., Jackson, B. L., Petit, R. S., Dustin, M. L. & Groves, J. T-cell triggering thresholds are modulated by the number of antigen within individual T-cell receptor clusters. *Proceedings of the National Academy of Sciences* **108,** 9089–9094 (May 2011).

57. Duguay, D., Foty, R. A. & Steinberg, M. S. Cadherin-mediated cell adhesion and tissue segregation: qualitative and quantitative determinants. *Developmental Biology* **253,** 309–323 (Jan. 2003).

58. Galush, W. J., Nye, J. A. & Groves, J. T. Quantitative Fluorescence Microscopy Using Supported Lipid Bilayer Standards. *Biophysical Journal* **95,** 2512–2519 (Sept. 2008).

59. Vacklin, H. P., Tiberg, F. & Thomas, R. Formation of supported phospholipid bilayers via coadsorption with β-D-dodecyl maltoside. *Biochimica et Biophysica Acta (BBA) - Biomembranes* **1668,** 17–24 (Feb. 2005).

60. Meseth, U., Wohland, T., Rigler, R. & Vogel, H. Resolution of Fluorescence Correlation Measurements. *Biophysical Journal* **76,** 1619–1631 (Mar. 1999).

61. Naji, A., Levine, A. J. & Pincus, P. Corrections to the Saffman-Delbrück Mobility for Membrane Bound Proteins. *Biophysical Journal* **93,** L49–L51 (Dec. 2007).

62. Chen, Y., Müller, J. D., So, P. T. & Gratton, E. The Photon Counting Histogram in Fluorescence Fluctuation Spectroscopy. *Biophysical Journal* **77,** 553–567 (July 1999).

63. Sackmann, E. & Bruinsma, R. F. Cell adhesion as wetting transition? *ChemPhysChem* **3,** 262–269 (Mar. 2002).

64. Kawanishi, J *et al.* Loss of E-cadherin-dependent cell-cell adhesion due to mutation of the beta-catenin gene in a human cancer cell line, HSC-39. *Molecular and Cellular Biology* **15,** 1175–1181 (Mar. 1995).

65. Zhang, F. & Low, H. Y. Ordered three-dimensional hierarchical nanostructures by nanoimprint lithography. *Nanotechnology* **17,** 1884 (Apr. 2006).

66. Mossman, K. D., Campi, G., Groves, J. T. & Dustin, M. L. Altered TCR Signaling from Geometrically Repatterned Immunological Synapses. *Science* **310,** 1191–1193 (Nov. 2005).

67. Zhang, J. *et al.* Actin at cell-cell junctions is composed of two dynamic and functional populations. *Journal of Cell Science* **118,** 5549–5562 (Dec. 2005).

68. Salaita, K. & Groves, J. T. Roles of the cytoskeleton in regulating EphA2 signals. *Communicative & Integrative Biology* **3,** 454–457 (Sept. 2010).

69. Choudhuri, K. & Dustin, M. L. *Unpublished Data* 2013.

70. Keppler, A. *et al.* Labeling of fusion proteins of O6-alkylguanine-DNA alkyltransferase with small molecules in vivo and in vitro. *Methods* **32,** 437–444 (Apr. 2004).

71. Coyle, M. P., Xu, Q., Chiang, S., Francis, M. B. & Groves, J. T. DNA-Mediated Assembly of Protein Heterodimers on Membrane Surfaces. *Journal of the American Chemical Society* **135,** 5012 –5016 (Mar. 2013).

72. Nakamoto, M. & Bergemann, A. D. Diverse roles for the Eph family of receptor tyrosine kinases in carcinogenesis. *Microscopy Research and Technique* **59,** 58–67 (2002).

73. Zelinski, D. P., Zantek, N. D., Stewart, J. C., Irizarry, A. R. & Kinch, M. S. EphA2 overexpression causes tumorigenesis of mammary epithelial cells. *Cancer research* **61,** 2301–2306 (Mar. 2001).

74. Orsulic, S & Kemler, R. Expression of Eph receptors and ephrins is differentially regulated by E-cadherin. *J Cell Sci* **113,** 1793–1802 (May 2000).

75. Fang, W. B. *et al.* Overexpression of EPHA2 receptor destabilizes adherens junctions via a RhoA-dependent mechanism. *Journal of Cell Science* **121,** 358–368 (Feb. 2008).